Biochemistry

pubs.acs.org/biochemistry Article

Mechanism of Catalysis by L-Asparaginase

Jacek Lubkowski,* Juan Vanegas, Wai-Kin Chan, Philip L. Lorenzi, John N. Weinstein, Sergei Sukharev, David Fushman, Susan Rempe, Andriy Anishkin, and Alexander Wlodawer

Cite This: *Biochemistry* 2020, 59, 1927−1945 Read Online

ACCESS | Metrics & More | Article Recommendations | Supporting Information

ABSTRACT: Two bacterial type II L-asparaginases, from *Escherichia coli* and *Dickeya chrysanthemi*, have played a critical role for more than 40 years as therapeutic agents against juvenile leukemias and lymphomas. Despite a long history of successful pharmacological applications and the apparent simplicity of the catalytic reaction, controversies still exist regarding major steps of the mechanism. In this report, we provide a detailed description of the reaction catalyzed by *E. coli* type II L-asparaginase (EcAII). Our model was developed on the basis of new structural and biochemical experiments combined with previously published data. The proposed mechanism is supported by quantum chemistry calculations based on density functional theory. We provide strong evidence that EcAII catalyzes the reaction according to the double-displacement (ping-pong) mechanism, with formation of a covalent intermediate. Several steps of catalysis by EcAII are unique when compared to reactions catalyzed by other known hydrolytic enzymes. Here, the reaction is initiated by a weak nucleophile, threonine, without direct assistance of a general base, although a distant general base is identified. Furthermore, tetrahedral intermediates formed during the catalytic process are stabilized by a never previously described motif. Although the scheme of the catalytic mechanism was developed only on the basis of data obtained from EcAII and its variants, this novel mechanism of enzymatic hydrolysis could potentially apply to most (and possibly all) L-asparaginases.

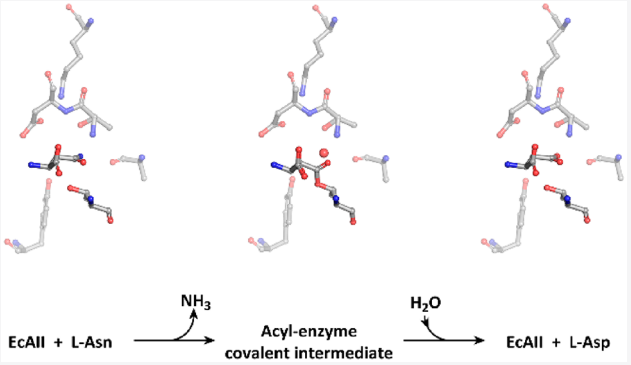

L-Asparagine amidohydrolases (L-asparaginases, EC 3.5.1.1) catalyze hydrolysis of L-Asn to L-Asp, with varied activities toward other substrates such as L-Gln, D-Asn, D-Gln, succinamic acid, etc. Furthermore, other compounds, including small amino acids (L-Ser, L-Ala, and L-Thr), citric acid, succinic acid, etc., bind with measurable affinity to the L-asparaginase active sites. L-Asparaginases are found in most bacteria and many higher organisms[1,2] but have not been studied as extensively as other hydrolases (i.e., Ser/Cys or Asp proteases).[3] L-Asparaginases from mesophilic bacteria form functional homotetrameric assemblies[4] with four chemically equivalent active sites.[5] In turn, many extremophiles or archaea encode L-asparaginases that function as homodimers, with only two equivalent active sites.[6] In either case, a single protomer consists of 320−350 amino acid residues. *Escherichia coli* encodes two weakly homologous homotetrameric L-asparaginases, encoded by genes *ansA* and *ansB*, and termed type I (EcAI, cytosolic) and type II (EcAII, secreted) L-asparaginase, respectively.

Interest in L-asparaginases greatly increased between the 1950s and 1970s, after discovery of their anticancer properties against various leukemias and lymphomas.[7] Since then, two L-asparaginases, from *E. coli* and *Dickeya chrysanthemi* (formerly known as *Erwinia chrysanthemi*, here abbreviated ErA), and their engineered variants, have become critical components of anticancer therapies, and even currently, their use is considered to be a strategy of choice due to their effectiveness and economic considerations.[8] Their anticancer properties stem from the fact that many leukemia or lymphoma cells carry a defective L-asparagine synthetase gene and are dependent on supply of plasma L-Asn.[9] Decreasing the level of L-Asn, an amino acid that is non-essential in normal cells, triggers signaling pathways in cancer cells, leading to their death. However, L-asparaginase therapy is not free of pitfalls, and side effects may include pancreatitis, hypercoagulability, liver dysfunction, and allergic reactions.[10] Consequently, much effort is focused currently on the development of variants with improved toxicity profiles.[11] In addition to medical applications, substantial quantities of L-asparaginases are used in food manufacturing.[12] When the significance of these enzymes in both medical and commercial applications and the apparently

Received: February 10, 2020
Revised: April 30, 2020
Published: May 4, 2020

simple chemical reaction catalyzed by them are taken into account, it is peculiar that no consensus about the general framework of the mechanism of catalysis has been reached to date.

Shortly after reports of the anti-lymphoma activity of guinea pig L-asparaginase[7] and the availability of high-quality preparations of EcAII,[13] multiple studies began to target the mechanism of catalysis.[14,15] Initially, several scenarios were evaluated, but some were quickly excluded.[16] By the late 1980s, only two general mechanisms of hydrolysis by L-asparaginases remained under consideration (Figure 1).

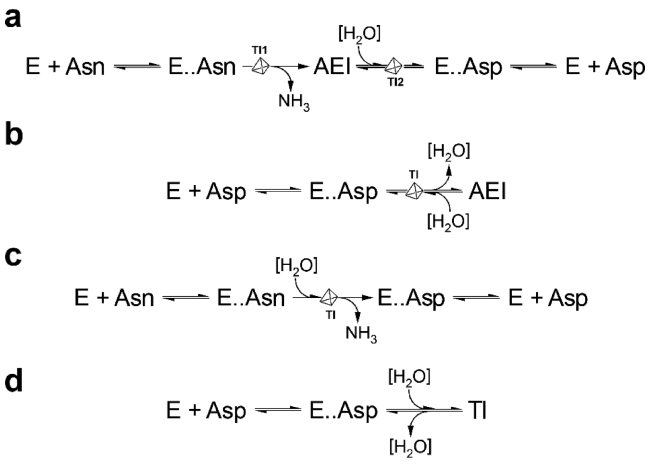

Figure 1. Schematic representation of two alternative mechanisms of catalysis by L-asparaginases. (a) The double-displacement mechanism represents a sequence of two nucleophilic substitutions, each associated with an energy barrier attributed to a tetrahedral intermediate (TI1 and TI2, respectively), separated by formation of the covalent acyl-enzyme intermediate (AEI). (b) Simplified scenario representing reversible oxygen exchange with the L-Asp substrate and a single tetrahedral intermediate (TI). (c) Single-displacement mechanism defined by direct nucleophilic substitution by a water molecule. (d) Variant of the reversible catalytic reaction with the L-Asp substrate.

According to the first mechanism (Figure 1a), a covalent acyl-enzyme intermediate (AEI) is formed following a nucleophilic attack by an enzyme residue on the carboxamide carbon of L-Asn (Figure 1a), with subsequent release of ammonia. Due to escape of ammonia from the active site, this catalytic step is irreversible. The second nucleophilic (and reversible) substitution is carried out by a water molecule and leads to the release of the second product, L-Asp, completing the catalytic cycle. Two tetrahedral intermediates, TI1 and TI2, are formed during each catalytic cycle. The catalytic reaction, a sequence of two nucleophilic substitutions, is often termed the double-displacement (or ping-pong) reaction. It was experimentally demonstrated[16] that L-Asp, the product of catalysis, is also a potent inhibitor, as well as a substrate when β-protonated. In the latter case, the catalytic reaction reflects oxygen exchange on the carboxylate carbon. The whole process is reversible, with formation of just a single tetrahedral intermediate, as illustrated by the simplified scheme shown in Figure 1b.

An alternative mechanism, the direct displacement, assumes just a single nucleophilic substitution by a water molecule (Figure 1c). In this scenario, both products, ammonia and L-Asp, are released simultaneously and the enzyme is not chemically engaged with the substrate. Similar to the first mechanism, hydrolysis of L-Asn would be irreversible, whereas the reaction with L-Asp would be reversible and represented by the equilibrium illustrated in Figure 1d. The main difference between the double- and single-displacement mechanisms is the presence of AEI in the former.

The results of previous biochemical and kinetic experiments did not determine unequivocally which of the two mechanisms is correct. Publication of the first two high-resolution structures, for EcAII and ErA,[5,17] both in complex with L-Asp, allowed a detailed description of the active site pocket. Those structural data supported the conclusion that under the double-displacement regimen, the first nucleophile could only be a Thr residue. Structural data did not, however, discriminate between the two mechanisms. Furthermore, an additional complication arose from the fact that two Thr side chains approach the product molecule in potentially catalytic positions.

The crystal structure of AEI was published in 1996, for the complex between L-Asp and the EcAII(T89V) variant.[18] The covalent bond between the carboxylate carbon of L-Asp and the hydroxyl oxygen of Thr12 was considered as proof of the double-displacement mechanism. That work, however, was not followed by further analysis of the catalytic reaction.

Notably, the conclusions mentioned above were questioned in at least two reports.[19,20] In one of them, the authors presented results of theoretical calculations that, in their interpretation, supported the single-displacement mechanism.[19] The authors of the second report, unable to detect and/or crystallize AEI from mixtures of catalytically deficient enzymes and L-Asn,[20] suggested that the creation of AEI[18] was due to an experimental artifact. Instead, they suggested the single-displacement mechanism of catalysis by L-asparaginases.

Here, we provide experimental and computational support for the double-displacement mechanism of hydrolysis by EcAII, which plausibly applies to the whole family of L-asparaginases. The evidence combines new results of crystallographic experiments (including structures of both AEI and TI complexes), the results of high-throughput activity screens for several variants of EcAII, and biochemical and biophysical analyses of selected variants of EcAII. The resulting description of the mechanism is in full agreement with the published biochemical, kinetic, biophysical, and structural data. We also explain possible causes of the alternative interpretations published previously.

MATERIALS AND METHODS

Reagents and Sequencing Services. The reagents L-Asn (catalog no. 51363), L-Asp (catalog no. 11189), sodium carbonate (Na_2CO_3, catalog no. 106395), sodium citrate dihydrate (catalog no. W302600), MES buffer sodium salt (catalog no. RES011M-A7), L-aspartic acid-3-hydroxamate (L-AHA, catalog no. A6508), isopropyl β-D-1-thiogalactopyranoside (IPTG, catalog no. PHG0010), glutaraldehyde (25% in H_2O, catalog no. G5882), trichloroacetic acid (catalog no. T9159), and 8-hydroxyquinoline (catalog no. H6878) were procured from Millipore-Sigma. All crystallization screens used in preliminary experiments were purchased from Hampton Research. Expression vector pET22b(+) (catalog no. 69744-3) was purchased from Millipore-Sigma, and the BL21 (DE3) expression cells (DE3) (catalog no. 230132) were obtained from Agilent Technologies. Nessler's reagent was prepared according to the protocol available at https://sites.chem.

https://dx.doi.org/10.1021/acs.biochem.0c00116
Biochemistry 2020, 59, 1927−1945

Table 1. Abbreviated Statistics for 11 Refined Structures Included in This Study (for more complete information, see Table S1)

Legend to Structure ID[a]	
1, EcAII(wt) (pH 7.3, formate), no ligands[b]	**2**, EcA(K162M) (pH 5, acetate), soaked with L-Asp
3, EcA(K162M) (pH 5, citrate), soaked with L-Asp	**4**, EcA(K162M) (pH 5.2, citrate), co-crystallized with L-Asp
5, EcA(K162M) (pH 5.2, acetate), soaked with L-Asp	**6**, EcA(K162M) (pH 5.6, acetate), soaked with L-Asp
7–**11**, crystals of EcA(T89V,K162T) grown under the same conditions and later cross-linked with glutaraldehyde, as described in Materials and Methods, and subsequently soaked for 20 s in solutions buffered at different pH values and containing the substrate specified: **7**, pH 4.7, L-Asp; **8**, pH 5.5, L-Asp; **9**, pH 6.2, L-Asp; **10**, pH 4.7, L-Asn; **11**, pH 5.5, L-Asn	

	1	**2**	**3**	**4**	**5**	**6**
space group	*I*222	$P2_12_12_1$	$P2_1$	$P2_1$	$P2_1$	*C*2
unit cell dimensions						
a, *b*, *c* (Å)	62.03, 71.19, 130.03	73.70, 125.91, 130.11	62.10, 125.97, 76.38	62.33, 126.12, 76.19	63.53, 123.97, 76.30	151.02, 62.29, 140.72
β (deg)	90	90	96.7	96.3	96.8	117.5
resolution (Å)	1.75	2.00	1.90	1.90	1.78	1.80
completeness (%)	94.4	95.7	96.5	97.6	93.0	91.1
R, R_{free}	0.182, 0.241	0.171, 0.235	0.149, 0.207	0.142, 0.190	0.136, 0.193	0.186, 0.196
status of the active sites[c]	empty	AEI and TI (A, C), AEI (B, D)	AEI and TI (B, C), AEI (A, D)	L-Asp (A), AEI (B, C), L-Asp and AEI (D)	L-Asp (A, C), AEI (B, D)	L-Asp (A–D)
no. of non-H atoms	2604	10815	10834	10844	11175	10895
no. of waters	236	965	1118	1026	1484	1250
average *B*-factor (Å^2)	32.7	28.7	32.3	22.1	29.5	25.8
bond rmsd (Å)	0.019	0.019	0.019	0.016	0.019	0.018
angle rmsd (deg)	2.30	2.23	2.29	2.06	2.22	1.960
PDB entry	6V23	6V2C	6V2G	6V24	6V25	6V26

	7	**8**	**9**	**10**	**11**
space group	*C*2	*C*2	*C*2	*C*2	*C*2
unit cell dimensions					
a, *b*, *c* (Å)	151.30, 62.41, 141.75	151.34, 62.54, 141.30	151.62, 62.43, 143.07	151.44, 62.59, 141.66	151.22, 62.58, 140.89
β (deg)	117.9	117.7	118.1	117.8	117.7
resolution (Å)	2.30	1.95	2.00	2.00	2.05
completeness (%)	97.6	97.6	98.9	92.1	93.3
R, R_{free}	0.160, 0.251	0.141, 0.189	0.142, 0.204	0.157, 0.209	0.152, 201
status of the active sites	AEI (A–D)	AEI (A–D)	L-Asp (A–D)	L-Asn (A–D)	L-Asn (A–D)
no. of non-H atoms	10155	11118	10400	10254	10373
no. of waters	613	1223	1018	599	679
average *B*-factor (Å^2)	35.6	14.7	30.0	29.2	28.1
bond rmsd (Å)	0.015	0.020	0.020	0.014	0.015
angle rmsd (deg)	2.07	2.18	1.92	1.89	1.92
PDB entry	6V27	6V28	6V29	6V2A	6V2B

[a]More details of the crystallization conditions are presented in Materials and Methods. [b]Legends illustrate the pH of the crystal environment prior to freezing, the type of buffer (i.e., citrate, formate, etc.), and the identity of the ligand and/or substrate. [c]Characters in parentheses represent chain IDs.

colostate.edu/diverdi/all_courses/CRC%20reference%20data/special%20analytical%20reagents.pdf. All other chemicals used were purchased at the highest available grade from different vendors.

DNA sequencing was performed by Macrogen Corp., using T7promoter and T7terminator universal primers. Additional reagents, tools, and kits used in cloning, extraction, and purification steps are identified along with a description of specific procedures.

All buffers were prepared fresh and used within 2 weeks. Nessler's reagent was used within two months of its preparation. The oxin/carbonate reagent was always prepared fresh prior to the assay. If not indicated otherwise, all other reagents or kits were prepared and used according to the manufacturer's recommendations.

Preparation of the Samples of Mutated EcAII. The DNA sequence encoding the EcAII gene with an N-terminal $(His)_6$ sequence was cloned into the commercial pET22b(+) vector (containing the secretion pelB leader), as described previously.[21] For expression, the vector was transformed into the *E. coli* JC2 strain [lacking three genes (*ansA*, *ansB*, and *iaaA*) encoding endogenous asparaginases]. After induction with isopropyl *β*-D-1-thiogalactopyranoside (IPTG; c_{final} = 1 *μ*M), expressions were carried out overnight (16–18 h) at 37 °C in the presence of ampicillin. After clearing by centrifugation and filtering, the supernatant was supplied with PMSF (c_{final} = 0.5 mM), phosphate buffer (c_{final} = 50 mM, pH 7.4), and sodium chloride (c_{final} = 0.3 M) and mixed with a Ni affinity resin (His60 Ni Superflow resin, Clontech). After being rocked for 3 h at 5 °C, the resin was isolated on a gravity

https://dx.doi.org/10.1021/acs.biochem.0c00116
Biochemistry 2020, 59, 1927–1945

Table 2. Catalytic Parameters of EcAII Variants Included in This Study

variant	k_{cat} (s^{-1})	K_m (mM)	variant	k_{cat} (s^{-1})	K_m (mM)
EcAII(wt)	25−54.4 [L-Asn][27,47,48]	0.035−0.12 [L-Asn][27,47,48]	EcAII(T89V,K162M)	0.00039 ± 0.00002 [L-AHA][a]	–
EcAII(T89V)	0.0021−0.0005 [L-AHA][44,47]	0.21−0.1 [L-AHA][44,47]	EcAII(D90K)	5.9 ± 0.3 [L-Asn][a]	–
	0.5 ± 0.05 [L-Asn][a]	–			
EcAII(K162M)	0.0035 ± 0.0003 [L-AHA][a]	–	EcAII(T12V)	0.0005 [L-AHA][47]	0.1 [L-AHA][47]
EcAII(Y25A)	0.54 [L-AHA][44]	0.24 [L-AHA][44]			

[a]Values determined in this study (see Figures 3b,c and 7).

column and washed as recommended by the supplier. Protein was eluted with 0.5 M imidazole and concentrated. The subsequent purification was carried out by means of size-exclusion chromatography on the S200 HP column (GE Life Sciences) in a buffer composed of 50 mM HEPES (pH 7.0) and 200 mM sodium chloride. The resulting pure preparation was concentrated to 10−20 mg/mL and either used immediately for crystallization experiments or frozen at −80 °C for future use.

Crystallization and Collection of X-ray Data. In all experiments, we used 8−12 mg/mL protein solutions in 50 mM Hepes buffer (pH 7.0) and 150 mM NaCl. All crystallizations were conducted in hanging drops formed from equal volumes of a protein solution and a precipitant solution. Crystals 1 were grown against a precipitant containing 0.1 M magnesium formate and 16% (w/v) PEG3350 (measured pH of 7.3). Prior to X-ray data collection, crystals were briefly soaked in the same solution but containing additionally 25% (v/v) glycerol. Crystals 2, 5, and 6 were grown using a precipitant containing 0.1 M sodium acetate buffered to pH 5, 5.2, and 5.6, respectively, 5 mM L-Asp, and 18−20% (w/v) PEG3350. Before being frozen, crystals were transferred to equivalent solutions also containing 25% (v/v) glycerol. Crystals 3 and 4 were prepared in two ways. In the first approach, the precipitant contained 0.17 M sodium citrate (pH 6) and 18% (w/v) PEG3350. The resulting crystals were soaked for 1 min in a mixture of 40% (w/v) PEG3350, 0.17 M sodium citrate (pH 5.0 for crystal 3 or pH 5.2 for crystal 4), and 5 mM L-Asp. Afterward, crystals were frozen and X-ray data were collected. In the second case, crystals were grown in the presence of 5 mM L-Asp, 18−20% (w/v) PEG3350, and 0.17 M sodium citrate buffered at pH 5 or 5.2. Prior to data collection, crystals were transferred to equivalent solutions, additionally containing 25% (v/v) glycerol. Crystals 7−11 were grown from a solution containing 0.17 M sodium citrate (pH 6) and 17−18% (w/v) PEG3350 and then transferred to an equivalent solution containing additionally 0.025% (w/v) glutaraldehyde. Optimal times of cross-linking (2−10 min) were determined individually for each crystal. Subsequently, crystals were briefly soaked (10−15 s) in solutions containing 40% (w/v) PEG3350, L-Asp or L-Asn, and 0.17 M sodium citrate at various pH values. A description of the substrate and pH for each crystal is given in Table 1.

All diffraction experiments were performed using an in-house conventional X-ray source, a Rigaku rotating anode MicroMax-007 HF generator operated at 40 kV and 30 mA, with a Cu Kα wavelength of 1.5418 Å. Images were recorded in a continuous mode with a Dectris Eiger 4M pixel detector. All measurements were conducted at 100 K. The images were processed and scaled using HKL3000.[22] Details of data collection and the processing statistics are listed in Table S1.

Structure Solution and Refinement. All structures were determined independently by molecular replacement with Phaser to minimize any possible bias.[23] We used protomer A of EcAII [Protein Data Bank (PDB) entry 3eca] as the search model, after removing ligand and solvent molecules, as well as the HR and ASFL sections (residues 10−31), and mutating Thr89 and Lys162 to Ala. In all cases, easily identifiable molecular replacement solutions were brought to a consistent origin and first subjected to rigid-body refinement at a resolution of 2.5 Å with Refmac5,[24] followed by several cycles of refinement of positions and isotropic atomic displacement parameters (Bf's) for non-H atoms, using the same program. In subsequent rounds of crystallographic refinement, the resolution was gradually extended to the limits of experimental data. Models were regularly inspected using Coot,[25] and appropriate corrections were introduced, including proper modeling of residues 89 and 162 and the ordered sections of ASFL. Ligand and solvent molecules were gradually incorporated in the structure based on difference electron density peaks. The near-final models were evaluated by the MolProbity server[26] and completed by applying additional corrections coupled with structural refinement. The statistics for the final structural models are listed in Table 1 and Table S1.

Measurements of Enzyme Kinetics. All measurements of absorption were performed with a NanoDrop One (Thermo Scientific). A comparison of readings obtained with the NanoDrop One and dual-cell Beckman DU530 spectrophotometer confirmed the equivalence of both protocols. For kinetic studies, we used discontinuous assays, described previously.[27]

Hydrolysis of L-Asn was examined by monitoring the formation of ammonia with Nessler's reagent. Reactions were conducted in 50 mM MES buffer (pH 6) with defined concentrations of the enzyme and L-Asn. In some experiments, a reaction mixture also contained L-Asp at a known concentration, to evaluate its effect on the rate of catalysis. At predetermined intervals, 40 μL aliquots were withdrawn and immediately mixed in microcentrifuge tubes with 40 μL of a 12% (w/v) solution of trichloroacetic acid (TCA) to stop the reaction. After the protein precipitate had been removed by centrifugation, 30 μL of the supernatant was mixed with 30 μL of Nessler's reagent and the absorption at 480 nm (A_{480}) was immediately recorded. To avoid extreme concentrations of ammonia (i.e., for a later stage of the assay and/or when a higher enzyme concentration was used), in some experiments the supernatant was first diluted with water prior to mixing with Nessler's reagent. To allow conversion of A_{480} values to concentrations of ammonia, we established the calibration curve based on a series of defined solutions of ammonium chloride in 50 mM MES (pH 6). The calibration curve was almost perfectly linear, consistent with the absorption coefficient of the product ε_{480} of 1115 ± 40 M^{-1} cm^{-1}, similar to the previously published value (ε_{480} = 1130 ± 50 M^{-1} cm^{-1}).[27] Seven independent measurements were taken at fixed

https://dx.doi.org/10.1021/acs.biochem.0c00116
Biochemistry 2020, 59, 1927−1945

intervals, and two extreme values were discarded prior to averaging.

In several assays, we monitored hydrolysis of an asparagine analogue L-aspartic acid β-hydroxamate (L-AHA) as the substrate at pH 5 (50 mM MES). The release of hydroxylamine was monitored via reaction with 8-hydroxyquinoline at basic pH, which leads to the formation of green oxindole dye (ε_{705} = 1.75 × 10^4 M^{-1} cm^{-1}).[28] As in the previous assay, 50 μL aliquots were withdrawn at regular intervals and mixed immediately with 25 μL of 6% TCA, to stop the reaction. After protein precipitates had been pelleted by centrifugation, 50 μL of the supernatant was mixed with 400 μL of the oxin/carbonate reagent (1 volume of 2% 8-hydroxyquinoline in ethanol with 3 volumes of 1 M Na_2CO_3). After samples had been boiled for 1 min (to develop the color) and cooled to room temperature, the values of A_{705} were recorded. A calibration curve was obtained from measurements of absorption values for a series of defined solutions of hydroxylamine hydrochloride. Table 2 shows the kinetic parameters determined in this study or obtained from the literature for the variants of EcAII examined in this work.

LC-MS Analysis of AEI Formation. Mass spectrometry data were acquired on an Agilent 6100 Series Quadrupole LC/MS System (Agilent Technologies, Inc., Santa Clara, CA) equipped with an electrospray source, operated in positive-ion mode. Separation was performed on a Zorbax 300SB-C3 Poroshell column (2.1 mm × 75 mm; particle size of 5 μm). Mass spectra were recorded across the range of m/z 300−2000. The ultraviolet signal was collected at 280 nm with a reference at 360 nm. Data acquisition and analysis were performed using OpenLAB CDS ChemStation Edition C.01.05.

Solutions containing 50 mM buffer (sodium acetate, pH 4−5.4; sodium cacodylate, pH 5.6−7.0; HEPES, pH 7.2−8.0), 3 μM EcAII(K162M), and 2.5 mM L-Asp were prepared immediately prior the mass spectrometry analysis.

Determination of Activity with Solution NMR. A determination of the rate of L-Asn hydrolysis by EcA(T89V) and EcA(D90T) variants was conducted using solution NMR spectroscopy with [^{13}C,^{15}N]L-Asn (Cambridge Isotope Laboratories) as a substrate. His_6-tagged variant enzymes were expressed in JC2 *E. coli* cells (1−2 L cultures) and isolated with two chromatographic steps as described above. All measurements were performed in 20 mM potassium phosphate buffer (pH 7.0) containing 5% D_2O. The 450 μL reaction mixture contained [^{13}C,^{15}N]-L-Asn and the enzyme mixed at different substrate:enzyme ratios, depending on enzyme activity, from 1:1 to 2500:1. NMR measurements were performed on a Bruker 600 MHz Avance III spectrometer equipped with a cryoprobe. Two-dimensional ^{1}H−^{13}C HSQC spectra were recorded at defined time intervals using standard pulse sequences, with spectral widths of 9615 Hz (^{1}H) and 10564 Hz (^{13}C). The spectra were processed using TopSpin (Bruker Biospin Inc.). Spectra of [^{13}C,^{15}N]-L-Asn and unlabeled L-Asp (at natural abundance) in the absence of enzyme were used as standards for signal assignment.

High-Throughput Activity Screening. Saturation mutations were introduced at nine different positions of EcAII (Ser19, Tyr25, Val27, Gly57, Ser58, Asp90, Lys162, Tyr250, and Glu283) using the GENEART Site-Directed Mutagenesis System (Invitrogen) according to the manufacturer's instructions. In all cases, the vector expressing EcAII(wt) was used as a template for mutagenesis together with the pair of oligonucleotide primers listed in Table S3. Analogous analysis for Gln59 was previously described.[21] All mutations were verified by DNA sequencing. For expression, genes of mutated EcAII variants were cloned in the expression vector [pET22b-(+)] containing the pelB leader sequence followed by the His_6 affinity tag. Subsequently, plasmids were transformed into *E. coli* strain BLR (DE3) (Novagen). Expression was monitored by Coomassie-stained sodium dodecyl sulfate−polyacrylamide gel electrophoresis, and examples are shown in Figure S2a. The activity of L-asparaginase was measured directly in supernatants from bacterial cultures according to protocols described above (see also ref 21). These measurements give only qualitative results and are not meant to be quantitative.

Electronic Structure Optimization and Energy Calculations. Electronic structure density functional theory (DFT) calculations, including optimizations to find the lowest-energy structures and single-point energies of the simulated systems, were conducted with the Q-Chem 4.4.2 quantum chemistry program.[29] Atomic coordinates for DFT calculations were taken from the crystal structure of EcAII in complex with L-Asp (PDB entry 6pac[30]). Given the high computational cost of DFT calculations, we selected a minimal subsystem of catalytic and essential structural amino acids near the active site, including residues G10, G11, T12, I13, G14, Y25, V27, G57, S58, Q59, H87*, G88, T89, D90, T91G, G113, A114, M115, R116*, K162, T165*, and T166* from chain "C" and residues V244, G245, N246*, G247, N248, A282*, and E283 from chain "D". Residues 87, 91, 116, 165, 166, 246, and 282 were included only to maintain structural integrity, and therefore, only the backbone atoms (side chains mutated to Gly) were used in the calculations. Missing hydrogen atoms were added on the basis of geometrical constraints for hydrogen bonding. In addition to the enzyme amino acids and the substrate, seven well-defined water molecules were included in the DFT model, including the two highly conserved waters, w1 (oxyanion hole) and w2 (catalytic water). Two independent calculations were performed for each of the two substrates, L-Asp (side chain protonated) and L-Asn. The positions of the substrate L-Asn atoms are the same as those of the L-Asp substrate, except that the side chain carboxylic acid is replaced with an amide. The total number of atoms for the subsystem with the L-Asn substrate is 341, while the total number of atoms for the subsystem with the L-Asp substrate is 340. Amino acids not connected to other residues, or at the end of a chain, were terminated at the C_α position (as a methyl group) to avoid spurious effects from charged termini such as COO^- and NH_3^+. α-Carbons of all protein residues were fixed to maintain the structural integrity of the active site during optimizations, except for residues G11, T12, I13, G88, T89, and D90, to minimize internal strain during nucleophilic attack or proton transfer. The two subsystems (L-Asp and L-Asn) were optimized at each of the reaction steps using three different functionals (B3LYP,[31−33] CAM-B3LYP,[34] and ωB97X-D3[35,36]) using the 6-31G(d) basis set as implemented in Q-Chem. The three different functionals were chosen to compare how different long-range corrections affect the reaction energetics. After optimization, single-point energies and partial point charges, computed from the electrostatic potential on a grid,[37−40] were calculated with the aug-cc-pVDZ basis set for every reaction step.

https://dx.doi.org/10.1021/acs.biochem.0c00116
Biochemistry 2020, 59, 1927−1945

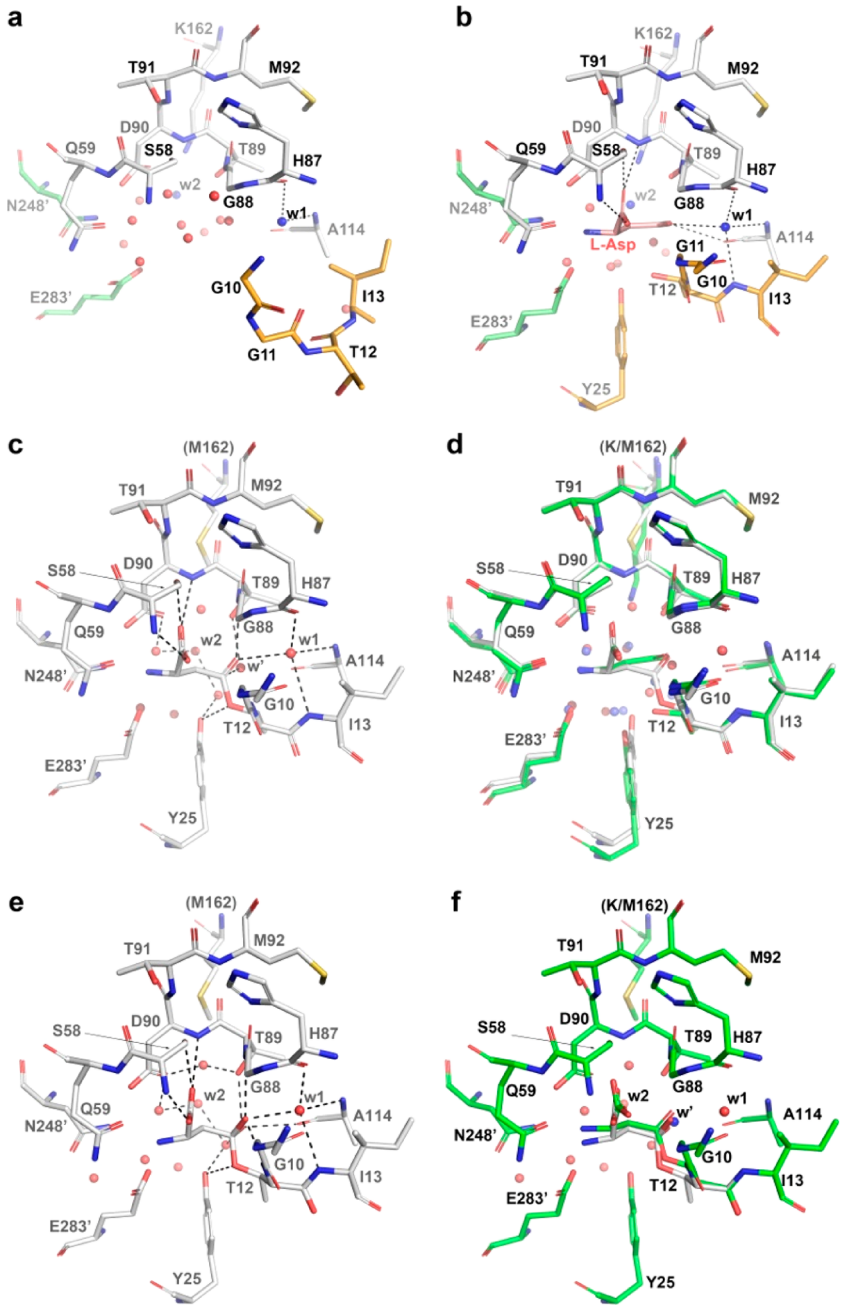

Figure 2. Active site of EcAII in different states. (a) Structure of the ligand-free active site of EcAII(wt), determined at a resolution of 1.75 Å at pH 7.3 (structure **1**). (b) Structure of the EcAII(wt):L-Asp complex (PDB entry 6pac, protomer A[30]). In both panels, gray and orange depict residues from the protomer forming a bulk of the active site pocket, while residues contributed by the second protomer are colored lime. Water molecules w1 and w2, invariant in all L-asparaginases, are shown as blue spheres, and all others are colored red. H-Bonds engaging the α-carboxyl group of the substrate and w1 are indicated by black dashed lines. (c) Structure of the covalent AEI, determined at 1.78 Å for crystals of EcAII(K162M) with L-Asp at pH 5.2 (structure **5**, protomers A and C). Despite the K162M mutation, w2 remains in the conserved position. Notably, an additional water molecule occupies the site of the NZ atom of Lys162. The H-bond network around w1 is indicated by the dashed lines. H-bonds, indicating stabilization of the α-carboxyl and ester groups of covalently bound substrate, are shown as black dashed lines. The H-bond network around the α-carboxylate of the substrate remains unchanged, compared to the noncovalent complex (panel b). A new water (or OH^-), labeled w′, is found in a position that was inaccessible in the noncovalent complex. (d) Superposition of the AEI-bearing active site (C atoms colored light gray and waters colored red) and the noncovalent EcAII:L-Asp complex (green C atoms and blue solvent atoms). (e) Structure of TI (structure **3**, protomers B and D). The H-bond network around w1, arranged in a nearly perfectly tetrahedral configuration, is indicated by dashed lines. (f) Complete model of the active site composed of TI (with carbon atoms colored gray) and AEI (carbon atoms colored green). In contrast to other water molecules (colored red), water w′ is colored blue. This water molecule is modeled at partial occupancy (0.6), matching that of AEI.

RESULTS

Active Site of EcAII. The primary goal of this project was to determine the mechanism of catalysis by EcAII at the molecular level by combining new results of structural and kinetic studies of the native enzyme and its mutated forms with the previously published ones. Currently, there are 28 structures of different variants of EcAII deposited in the PDB. In this work, we provide 11 additional, refined structures

https://dx.doi.org/10.1021/acs.biochem.0c00116
Biochemistry 2020, 59, 1927−1945

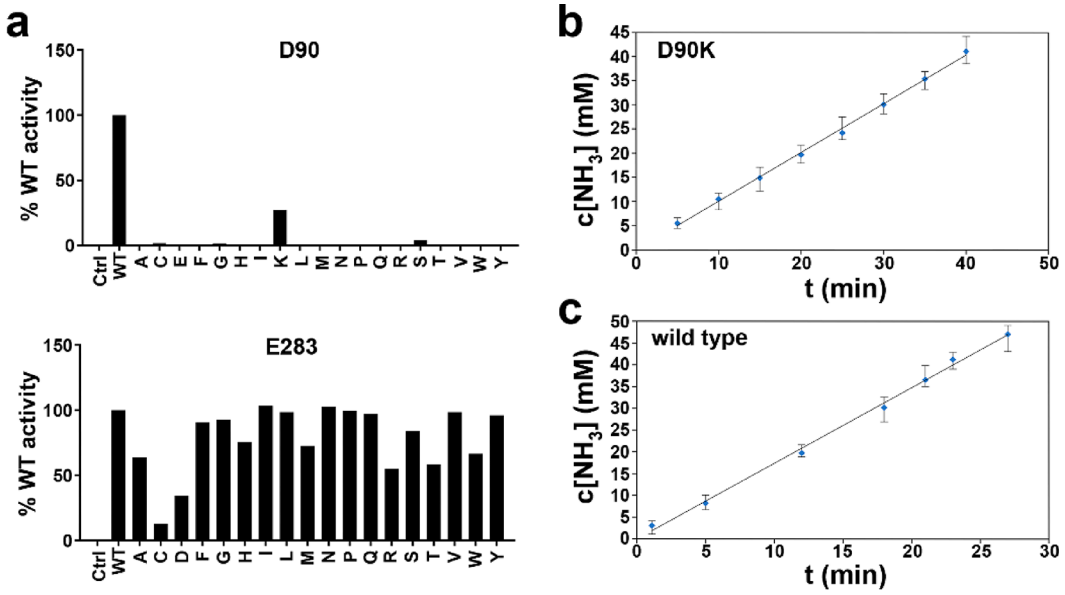

Figure 3. Enzymatic activities of representative EcAII variants. (a) Relative activities of EcAII variants in which either Asp90 or Glu283 was substituted by all other amino acids, with AHA used as the substrate. The activity of each variant is shown as bars, relative to the activity of the wild type enzyme taken as 100%. The negative control indicates use of an empty expression vector. (b and c) Progress curves for L-Asn hydrolysis at pH 7 by EcAII(D90K) and EcAII(wt), respectively. In each panel, the individual values (○) are averages from four independent measurements. The range of values, for each data point, is illustrated by vertical error bars. The error of time measurement is estimated as ±2 s. Reactions were conducted in 100 mM Hepes buffer, with starting concentrations of L-Asn, EcAII(D90K), or EcAII(wt) of 100 mM, 25 μM, or 0.15 μM, respectively. In the case of EcAII(D90K), the trend of the progress curve is linear [$c(NH_3)$ (mM) = 0.0167 × t (s)], with the Pearson product coefficient equal to 0.9979 and an estimated turnover time for hydrolysis of 0.17 s. For EcAII(wt), the linear progress follows the equation $c(NH_3)$ (mM) = 0.029 × t (s), with the Pearson product coefficient equal to 0.9979 and an estimated turnover time of 0.02 s.

of three different variants of EcAII. They include the structure of ligand-free EcAII(wt) (structure 1) and five structures of each of the two variants, EcAII(K162M) and EcAII-(T89V,K162T). These variants catalyze hydrolysis of the substrate at an extremely low rate. The basic characteristics of these structures are listed in Table 1.

Previously, several structures of L-asparaginases were determined from crystals of the enzyme grown in the absence of a substrate; however, in all cases, a molecule of either L-Asp or a buffer was found bound to the active site.[5,41] Here, crystals of EcAII(wt) were grown in the solution buffered by sodium formate at pH 7.3, and no multiatom assemblies were found in the active site pocket. Therefore, structure 1 (Figure 2a) represents the best currently available reference model for ligand-free EcAII and provides an unbiased description of the water network in such an active site. This structure is important during evaluation of conformational changes associated with substrate binding that, in turn, are central to understanding the kinetic process at the molecular level.

Because the structural features of L-asparaginases have been extensively described in the past,[42,43] this report focuses solely on an analysis of the active site pocket. The relationship among the four protomers forming the biological assembly of L-asparaginase and the location of four chemically identical active sites are illustrated in Video 1.

The active site of EcAII exists in one of two structurally distinctive states. The first state (Figure 2a) represents a ligand-free active site of EcAII(wt). The second state is exemplified by the complex between EcAII(wt) and β-protonated L-Asp (Figure 2b). In addition, Figure S1 depicts a superposition of the EcAII(wt):L-Asp complex and the complex between an inactive variant EcAII(T12V) and L-Asn. Combined, these representations provide a comprehensive overview of the active site pocket. Importantly, modes of binding of the L-Asn and L-Asp molecules are nearly indistinguishable (Figure S1). A comparison of panels a and b of Figure 2 shows that residues contributed by the hinge region (HR) and the active site flexible loop (ASFL) undergo dramatic conformational changes upon substrate binding. In L-asparaginases, HR is a highly conserved Gly-rich octapeptide, defined by the pattern GGTxyGGG (where x is an Ile or a Leu and y is an Ala or a Gly). In EcAII, HR is represented by the sequence G^{10}GTIAGGG^{17}. The ASFL in EcAII spans residues D^{18}SATKSNYTVGKVG^{31}, although there is no precise boundary between HR and ASFL. Except for these two fragments, the active sites of these enzymes are quite rigid and well-conserved across different L-asparaginases. The distribution of solvent molecules varies somewhat between different structures or even different active sites in the same structure, except w1 and w2, colored blue in panels a and b of Figure 2. However, the active sites, whether ligand-free or in complexes, are always well hydrated with water molecules forming a network of H-bonds that is suitable for efficient transfer of proton(s) between distant regions of the pocket. Furthermore, analysis of the active sites by molecular dynamics (not shown) suggests that the space available to solvent molecules may be larger than experimentally established.

In the past, many residues of EcAII were mutated and the expressed enzymes were studied by either functional or kinetic assays.[18,27,44−48] A summary of selected kinetic parameters for a wide range of EcAII variants is presented in Table 2 and Table S2. Combined with structural data, the kinetic parameters facilitated identification of five residues (Thr12, Tyr25, Thr89, Asp90, and Lys162) as being critical for catalysis. Thus, any description of a putative catalytic mechanism must incorporate at least those residues. Several

https://dx.doi.org/10.1021/acs.biochem.0c00116
Biochemistry 2020, 59, 1927−1945

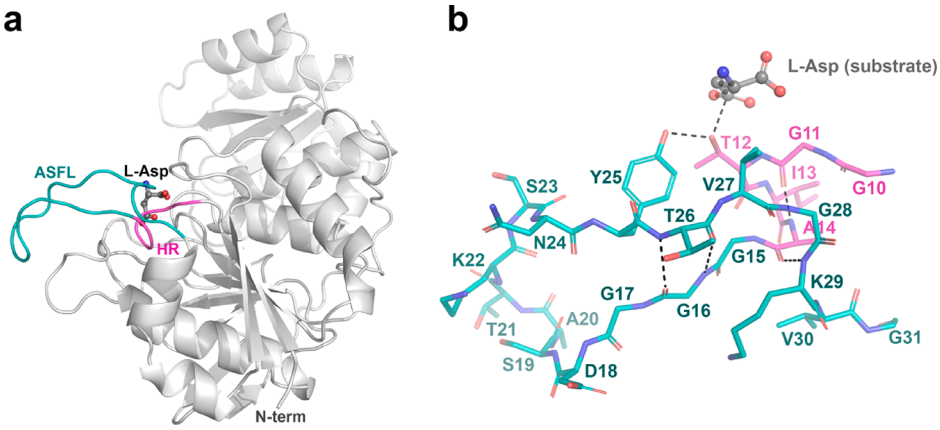

Figure 4. Representation of ASFL. (a) Ribbon representation of the EcAII protomer (colored mostly light gray) in which HR and ASFL, both in the *cat*+ conformation, are colored magenta and cyan, respectively. A molecule of L-Asp occupying the active site pocket is also shown in a ball-and-stick representation. The C-terminus of the enzyme, located on the back face of the upper part of the molecule, is not visible. In the *cat*+ conformation, ASFL does not form stabilizing interactions with the rest of the enzyme. (b) More detailed representation of HR (magenta) and ASFL (cyan), both in *cat*+ conformations. Stabilizing interactions are indicated with black dashed lines. Four putative H-bonds, Ile13(O)−A14(N), A14(O)−K29(N), G16(N)−T26(O), and G16(O)−T26(N), can be identified within the HR−ASFL fragment. Two additional interactions involving the catalytic Thr12 and Tyr25 and the substrate molecule have near-optimal geometry.

other residues are important for substrate binding, the most significant of which are Ser58 and Asp90 (see Figure 2b, Figure S1, and Table S2); a few additional residues, i.e., Gln59, Asn248, and Glu283, may also influence substrate binding. Some residues appear to play a role in defining substrate specificity, but that subject is not discussed here. Compared to classical kinetic studies, data from the high-throughput screening are only semiquantitative and lack information about the role of each specific position in substrate binding (or K_m). However, they illustrate well the significance and indispensability of each residue for the catalytic reaction (k_{cat}). In this work, we extended functional studies of EcAII by completing a high-throughput analysis of nine residues (Ser19, Tyr25, Val27, Gly57, Ser58, Asp90, Lys162, Tyr250, and Glu283).

The results obtained for Asp90 and Glu283 are shown in Figure 3a, and the remaining ones are listed in Materials and Methods.

As an example, Figure 3a highlights the critical role of Asp90 for catalysis. However, it is also apparent that the chemical composition of the side chain may be less important than its proper location and the ability to efficiently shuttle protons, because the D90K variant retains significant enzymatic activity (see Table 2). The results from classical kinetic studies (see Table S2) further show a critical role of this residue in substrate binding. Alerted by the outcome of the high-throughput assay for the D90K variant, we subjected it to more rigorous analysis in parallel to EcAII(wt). The results are shown in panels b and c of Figure 3. We confirmed that the EcAII(D90K) variant retains a significant degree of catalytic activity and provide a rationale of this finding in the Discussion. In contrast, the results obtained from the screen of Glu283 suggest that this residue is not critical to catalysis, which agrees with its low degree of conservation among L-asparaginases.[49,50] However, kinetic characterization of Glu283 variants indicates that in EcAII this residue contributes to substrate binding, which is understandable from structural studies (Figure 2b and Figure S1).

Binding a substrate molecule induces dramatic conformational changes in two adjacent regions in the EcAII active site, HR and ASFL. In a majority of L-asparaginase structures, HR accommodates one of two stable conformations (Figure 2a,b), with the last three Gly residues structurally ordered in only one of them. In the noncatalytic conformation (*cat*−), observed in the absence of a substrate, the side chain of Thr12 points away from the active site and the main chain atoms of HR do not interact with the substrate. In the catalytic (*cat*+) conformation of HR, observed for complexes with a substrate, Thr(O_γ) and the backbone amides, i.e., Ile13(N) in EcAII, point toward the active site. Both the *cat*− and *cat*+ conformations and/or states are stable. In contrast, ASFL extending from Asp18 to Gly31 in EcAII remains in a disordered state (*cat*−) in the ligand-free enzyme. While some previous reports described stable, unique conformation(s) of ASFL,[50,51] revisiting these structures shows that stabilization of such conformations can be attributed to crystal contacts. Upon substrate binding, ASFL assumes the unique *cat*+ conformation (Figure 2b), in which the hydroxyl group of Tyr25 (contributed by ASFL) forms an H-bond with Thr12(O_γ) from HR. The HR and ASFL regions in EcAII, both in the *cat*+ conformation, are illustrated in Figure 4. In some X-ray structures, despite the presence of a substrate in the active site, ASFL remains largely disordered[30] (PDB entries 6paa and 6pa9).

Such examples often describe crystals subjected to transient soaking in substrate-containing solutions. This effect is mostly a consequence of predefined crystal contacts that prevent rearrangement of ASFL to the *cat*+ conformation or from the absence of interactions stabilizing the *cat*+ state of ASFL. Therefore, interpretation of such results requires the utmost caution. As indicated above, both Thr12 and Tyr25 are critical for catalytic reaction.

Lastly, neither HR nor ASFL contributes significantly to substrate binding, as confirmed by kinetic studies (Table 2 and Table S2). As shown in Figure 4b, HR forms a single interaction with a substrate molecule that is already bound to the active site pocket, and ASFL also forms only a single H-bond with HR [Thr12(OH) with Tyr25(OH)]. While there are H-bonds with suboptimal geometry within ASFL or HR, neither region forms additional interactions with the rest of the enzyme.

https://dx.doi.org/10.1021/acs.biochem.0c00116
Biochemistry 2020, 59, 1927−1945

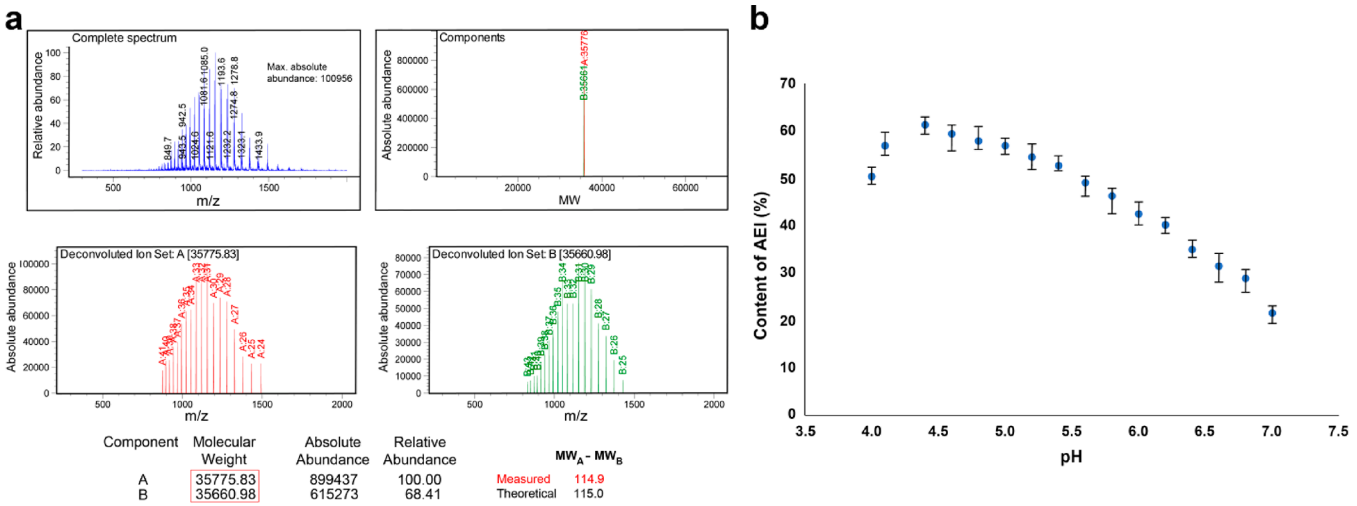

Figure 5. LC-MS analysis of the EcAII(K162M):L-Asp mixture at various pH values. (a) Example of a raw LC-MS result acquired for a sample at pH 4.6. The top left panel depicts the detected ions, and the panels below show deconvolution into two clearly identified molecular weights (MWs). Peak B represents the MW of the enzyme, and peak A the MW of AEI. The difference (indicated in red below) corresponds to the MW of an acyl-enzyme intermediate. (b) Change in the content of AEI (cAEI) with pH. Values of cAEI were calculated according to the formula [cAEI = abundance of AEI (%)]/{[abundance of AEI (%)] + [abundance of EcAII(K162M) (%)]}. The abundances of AEI and EcA(K162M) were measured in triplicate, and the average values, together with the ranges (error bars), are shown in the plot.

Covalent AEI: Evidence of a Double-Displacement Mechanism. The oxygen exchange reaction in L-Asp catalyzed by EcAII is reversible (Figure 1b). Using LC-MS, we studied this equilibrium for a series of solutions containing fixed quantities of the catalytically deficient EcAII(K162M) variant and L-Asp in the pH range of 3−7 (see Figure 5). We used a catalytically deficient variant because the equilibrium illustrated in Figure 1b for EcAII(wt) is dramatically shifted toward noncovalent specimens. The same experiments were performed using two different variants, EcAII(T89V) and EcAII(T89V,K162M), leading to equivalent results. In the absence of L-Asp, only one analyte, EcAII(K162M), was detected. However, addition of the substrate resulted in formation within 1 min of an additional covalent specimen, with a molecular weight (MW) corresponding to that of the covalent AEI (Figure 5a). The profile shown in Figure 5b indicates that decreasing the pH from 7.0 to 4.4 shifts the equilibrium toward AEI. When the pH drops below 4.4, however, the equilibrium shifts slightly back toward the noncovalent complex. These results allow for two conclusions. First, the maximum AEI content is observed at pH ∼4.5, suggesting that the acidity of the side chain carboxyl group of a substrate is significantly lower than that of a water solution (pK_a = 3.9[52]), and a significant relative content of AEI (>20%) is detected even at pH 7 (Figure 5b). These observations indicate that oxygen exchange on the β-carboxyl group of L-Asp is an enzymatic process. In the absence of the enzyme, this exchange would be orders of magnitude slower at pH 7.[16] Because the oxygen exchange process involves formation of AEI, these data directly and unambiguously support the double-displacement mechanism. Also, the profile presented in Figure 5b is easily explained in the context of the complete mechanism presented below. The initial shift of equilibrium toward AEI (observed with a decrease in pH from 7 to 4.4) is primarily associated with an increasing concentration of β-protonated L-Asp and with a decreasing rate of deacylation (AEI → E + S). However, at lower pH values, these effects are countered by increasing the amount of the protonated α-carboxyl group of L-Asp. Whereas these experiments unequivocally record formation of covalent AEI, they do not reveal the identity of the nucleophile.

To address this problem, we determined several structures of two variants, EcAII(K162M) and EcAII(T89V,K162T), for which LC-MS data indicated the presence of AEI in the active site pocket. To answer the previous criticism indicating that growing crystals over a long period could lead to experimental artifacts due to processes not catalyzed by the enzyme,[20] these experiments followed protocols that emphasized the enzymatic nature of the reaction, i.e., chemical changes leading to final structures happening at rates far exceeding those of non-enzymatic processes. The structure of active sites determined in one such experiment for EcAII(K162M), structure **5**, is shown in Figure 2c. An agreement between the refined structure and the electron density maps is shown in Figure S7a. This result not only supports the double-displacement mechanism of catalysis by EcAII but also unambiguously identifies Thr12 as the nucleophile. Inspection of Figure 2c shows that AEI is engaged in an extensive set of well-defined interactions with the active site residues. A comparison of structures determined for the noncovalent complex and AEI (Figure 2d) shows that conformational changes of either the substrate or the active site residues are minimal. The largest difference is observed for the side chain of the substrate that, after conversion to AEI, rotates around the C_β−C_γ bond by ∼90° and shifts slightly toward HR. As we have recently shown[30] (PDB entries 6paa and 6pa9 and Figure S1), EcAII(T12V) does not form an alternative intermediate through acylation of Thr89 in the presence of L-Asp. Instead, the substrate was invariantly noncovalently bound to the mutated enzyme in a mode illustrated in Figure 2b and Figure S1. These results provide strong evidence that Thr89 lacks the ability to act as the primary nucleophile.

Like a water molecule, the hydroxyl group of threonine is a weak nucleophile and Thr12 is not directly assisted by a basic residue capable of enhancing its nucleophilic properties, unlike in the previously observed case of Ser/Cys proteases.[3] It is

https://dx.doi.org/10.1021/acs.biochem.0c00116
Biochemistry 2020, 59, 1927−1945

therefore imperative to explain how Thr12 acquires the capacity to initiate a nucleophilic attack, which is one of the long-standing puzzles associated with L-asparaginases. We suggest that the precise placement of three atoms, the hydroxyl oxygen of Thr12, the C_γ atom of the substrate, and the hydroxyl oxygen of Tyr25, plays a prominent role. The substrate molecule bound to the active site pocket is strongly restrained by a network of interactions (Figure 2b,c,e). We showed earlier that neither HR (Thr12) nor ASFL (Tyr25) contributes significantly to substrate binding. While HR and ASFL may undergo spontaneous low-energy transitions between *cat*− and *cat*+ states even in the absence of a substrate, stabilization of HR(*cat*+) can be achieved by an interaction between Thr12(O_γ) and Asx(C_γ) only with substrate bound to the active site pocket. The precisely positioned Thr12 serves as an "anchor" for the hydroxyl group of Tyr25, which leads to stabilization of the ASFL(*cat*+) conformation. We reported earlier that in such an arrangement the O_γ atom of Thr12 approaches the C_γ atom of the substrate along the most favorable trajectory for a subsequent nucleophilic attack.[30] In an attempt to understand the basis of an attraction between these two atoms, we have evaluated the partial charges for all of the atoms in the substrate-occupied active site of EcAII based on the electrostatic potential from quantum mechanical density functional theory (DFT) calculations (see Materials and Methods).

Figure 6 illustrates two subsets of data, including only non-H atoms of the substrate molecules and the side chain of Thr12.

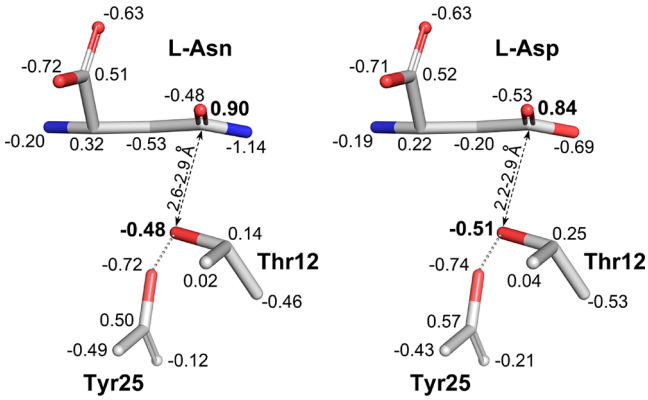

Figure 6. Partial atomic charges for EcAII substrate molecules computed with DFT. Values of partial charges were calculated for the complete active site pockets, occupied by either L-Asn or L-Asp. Partial charges computed from the electrostatic potential on a grid after DFT single-point calculations with the CAM-B3LYP functional and aug-cc-pVDZ basis set (see Materials and Methods). In this figure, the calculated charges are shown for only non-H atoms of the substrates and for the side chains of Thr12 and Tyr25. Charges on the atoms forming a covalent bond in AEI are shown in a larger bold font. The dashed arrow indicates the trajectory of a nucleophilic attack and is accompanied by the ranges of distances between Thr(O_γ) and L-Asx(C_γ) observed in crystals of various noncovalent complexes of substrates with EcAII. The gray dotted line indicates the H-bond that is utilized during extraction of a proton from Thr12.

Although theoretically derived partial charges depend on the employed protocol, values calculated here for L-Asn are in good agreement with those derived differently and reported previously.[53,54] Quite striking is the large partial positive charge (+0.9*e*) of the C_γ atom adjacent to the electron-rich Thr12(O_γ). This configuration most likely induces a subsequent nucleophilic attack, and the electrostatic forces can support the transition from HR(*cat*−) to HR(*cat*+). Furthermore, the rearrangement of HR leads to the formation of two new H-bonds around w1 (Figure 2a,b), fully defining its coordination from the H-bond pattern. This water molecule accepts two protons (via H-bonds) from the backbone amides of Ile13 and Ala114 and donates one proton to the backbone carbonyl of His87 and the second to the O_δ atom of the substrate or AEI. The latter interaction further restrains the substrate and subsequently stabilizes the negatively charged tetrahedral intermediates (TI1 and TI2). At this point, a stage for the nucleophilic attack is established. Without additional structural changes, a suboptimal catalysis begins, albeit at a rate ∼100-fold slower than that observed for EcAII(wt) [based on the rate observed for EcAII(Y25A) (Table 2)].

Stabilization of ASFL in the *cat*+ conformation establishes conditions that fully support the catalytic process. ASFL now places Tyr25(OH) in the position that establishes an H-bond-based connection of Thr12(O_γ) with a network of active site water molecules. As we indicated earlier, all events mentioned above are completely dependent on the precise and unique relative placement of the three critical atoms. Formation of an H-bond network allows for efficient extraction of the H atom from the hydroxyl group of Thr12. In principle, that goal can be achieved without any involvement of Tyr25, with an additional water replacing the missing Tyr25(OH). However, additional motions of these atoms would likely destabilize the interactions, resulting in a lower catalytic efficiency (∼100 times).

Earlier, we emphasized the importance for substrate binding of the interactions between the α-carboxyl group of the substrate and a region of the active site around Ser58 and Asp90, which indeed was repetitively shown to be critical. In such an arrangement, however, two negatively charged carboxyl groups (the α-carboxyl of the substrate and the side chain of Asp90) are placed quite close to each other (∼3.5 Å), an observation that seems counterintuitive with respect to the observed high affinity of EcAII for a substrate (see Table S2). This difficulty may be resolved if, concomitant to binding the substrate, Asp90 becomes protonated. We suggest that this process is accomplished by the transfer of a proton from Thr12 via precisely placed Tyr25(OH) and a network of active site water molecules, illustrated in panels c and e of Figure 2. In such a scenario, a system of two adjacent carboxyl groups acts as a "proton sink", increasing the efficiency of the first nucleophilic displacement. We select Asp90 over the substrate's α-carboxylate as the destination for the proton based on both our structural analysis (see Materials and Methods) and its predicted lower acidity. Furthermore, we suggest that Asp90 remains in a protonated state until the late stages of the catalytic reaction, because that assures stable binding of the substrate and TI or AEI. In conclusion, we should consider Asp90 as a distant general base that enhances the nucleophilic properties of Thr12. It is also conceivable that protonation of Asp90 increases the acidity (i.e., decreases the pK_a) of the adjacent Lys162. In this scenario, Tyr25 becomes a proton conveyor. Independent support for such an interpretation comes from the high-throughput screen. Investigation of mutations of position 25 (Figure S2) indicates that the only other residue retaining significant catalytic activity (∼25%) is Lys. Among all 20 amino acids, only lysine can uniquely provide a group (NH_3^+, allowing for efficient proton transfer) at nearly the same site as tyrosine, as the lengths of

https://dx.doi.org/10.1021/acs.biochem.0c00116
Biochemistry 2020, 59, 1927−1945

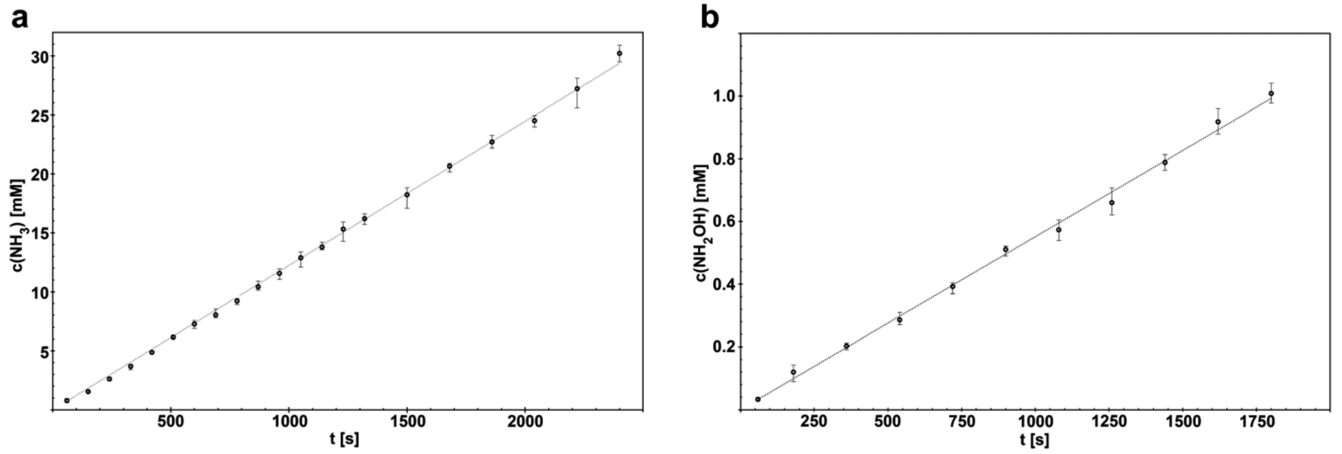

Figure 7. Progress curves for substrate hydrolysis by EcA(T89V). In each panel, the individual values (○) are averages from five independent measurements. The range of values, for each data point, is illustrated by vertical error bars. The error of time measurement is estimated to be ±2 s. (a) Reaction with L-Asn at pH 6. The reaction was conducted in 50 mM MES buffer (pH 6) containing 24.8 μM EcAII(T89V) and L-Asn ($c_{\text{L-Asn},0}$ = 175 mM) at time zero. The total consumption of the substrate was 17.5% of an initial concentration, $c_{\text{L-Asn},0}$. The trend of the progress curve is linear [$c(NH_3)$ (mM) = 0.0122 × t (s)], with the Pearson product coefficient equal to 0.9994. The estimated turnover time for this hydrolysis is 2.0 s. (b) Hydrolysis of L-AHA at pH 5 in the presence of L-Asp. The reaction was conducted in 50 mM MES buffer (pH 5) containing EcAII(T89V) at a concentration 9.2 μM, L-AHA ($c_{\text{L-AHA},0}$ = 53.5 mM), and L-Asp ($c_{\text{L-Asp}}$ = 1 mM) at time zero. The total consumption of the substrate was 1.9% of $c_{\text{L-AHA},0}$. The trend of the progress curve is linear [$c(NH_2OH)$ (mM) = 0.0006 × t (s)], with the Pearson product coefficient equal to 0.9968. The calculated turnover time is 15.8 s.

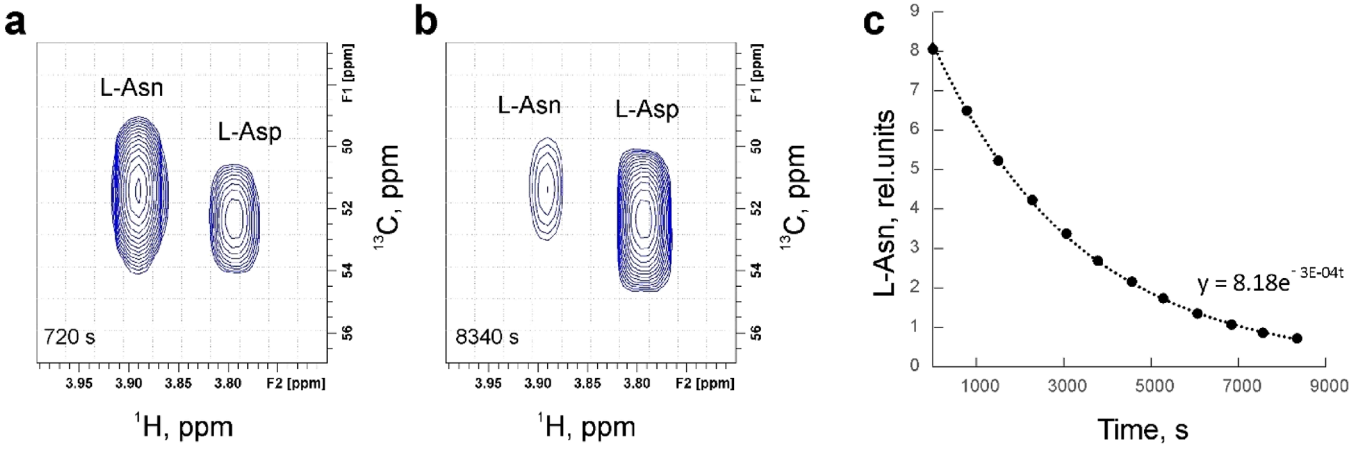

Figure 8. Measurement of the EcA(T89V) turnover rate using solution $^1H-^{13}C$ NMR. Characteristic $^1H^{13}C$ peaks of [^{13}C,^{15}N]-L-Asn and [^{13}C,^{15}N]-L-Asp at (a) 12 and (b) 139 min of reaction progress. (c) Time course of [^{13}C,^{15}N]-L-Asn signal decay fitted with a single exponential. The His_6-tagged variant enzyme was expressed in JC2 cells and purified as described in Materials and Methods. The reaction was monitored on a Bruker 600 MHz spectrometer at 25 °C. The 450 μL reaction mixture contained 0.5 μM purified EcA(T89V) and 1.25 mM [^{13}C,^{15}N]-L-Asn at time zero in 20 mM phosphate buffer (pH 7.0).

the side chains of Lys and Tyr are comparable. Furthermore, the pK_a values of Tyr(O**H**) and Lys(N**H**$_3^+$) are comparable [10.5 (from ref 52)].

Extraction of a hydrogen from Thr12 is simultaneous with a decrease in the distance between Thr12(O_γ) and the C_γ atom of the substrate and rearrangement of an electronic structure on the carboxamide group. Hybridization of the C_γ atom changes from sp^2 to sp^3, leading to TI. Tetrahedral intermediates are central to both displacements. In the acylation reaction, TI mediates the transition of a noncovalent enzyme:substrate complex to covalent AEI. In the deacylation reaction, it separates AEI from the enzyme:product complex. These states also define the energy barriers associated with both reactions.

Both LC-MS and crystallographic experiments unambiguously show formation of AEI and identify Thr12 as the primary nucleophile. In this study, we also completed an additional series of kinetic studies targeting the question of a possible "unusual" burst effect (i.e., long time effect lasting a few minutes) accompanying L-Asn hydrolysis by EcAII described previously.[18] This effect was subsequently questioned.[20] In the optimized assays monitoring hydrolysis of either L-Asn or AHA, we found that both reactions progress linearly over time and no "unusual" burst effect is observed (Figure 7). Similar results were obtained for two other variants, EcAII(K162M) and EcAII(T89V,K162T) (Materials and Methods). Throughout these studies, however, we found that EcAII(T89V) is only 80−150 times less active than the wild type enzyme, i.e., ∼100 times more active than previously reported.[18,44] Table 2 summarizes kinetic data for the EcAII variants studied here that were either determined in this study or taken from the literature.

https://dx.doi.org/10.1021/acs.biochem.0c00116
Biochemistry 2020, 59, 1927−1945

We corroborated this result by an independent NMR experiment in solution, monitoring formation of the L-Asp product, with the rate of L-Asn hydrolysis by EcA(T89V) evaluated using [^{13}C,^{15}N]-L-Asn as the substrate. Free L-Asn and L-Asp (product) have discernible ^{1}H^{13}C spectral peaks (Figure 8a,b), allowing us to trace their ratio in the course of the reaction. Figure 8c shows the time course of L-Asn decay in the mixture with purified EcA(T89V) at an initial 1:2500 enzyme:substrate molar ratio. Exponential fitting of the L-Asn data indicated 3.3×10^{3} s as the characteristic time of the exponent, which converts to the overall initial hydrolysis rate of 3.05×10^{-7} mol/s. With the account of the molar ratio, this rate corresponds to 1.64 s per catalytic cycle. Because the substrate is present at a saturating concentration (1.25 mM; $K_m \sim 40$ μM), we may conclude that the k_{cat} for this variant is 0.39 s^{-1}. We have also characterized the catalytic rate of the EcA(D90T) variant in a similar experiment. To detect the change in the labeled substrate, we had to use it at a 1:1 molar ratio with the enzyme (0.13 mM each). Within an 80 min reaction time span, we detected an ∼11% decrease in the [^{13}C,^{15}N]-L-Asn concentration, which led to the estimation of the turnover time as ∼9000 s at a given substrate concentration. We found that EcA(D90T) does not bind L-Asp effectively because most of the substrate remained unbound. We concluded that the low binding affinity is the main reason for the extremely slow reaction rate. We also found that the EcA(D90T,K162T) variant does not bind the substrate and is virtually inactive, based on a 16 h observation (data not shown). This confirms that Asp90 is a critical residue for substrate binding. The lack of observed "unusual" burst kinetics, or any burst effect, does not preclude the existence of the double-displacement mechanism. In general, burst kinetics could be observed only if the rate of the second displacement was significantly slower than the rate of the first displacement, leading to detectable accumulation of AEI. While the second displacement is the same in catalytic reactions with L-Asn and L-Asp, the energy barriers associated with the first displacement are significantly higher in the case of the former substrate (resulting in lower rates of displacement). Thus, the rate of catalytic hydrolysis of L-Asn by EcAII is controlled by the rate of the first displacement reaction, in agreement with results of earlier kinetic studies of various substrates.[55] As a result, no "unusual" burst effect is observed and AEI is not detected by either LC-MS or structural methods. By contrast, with the L-Asp substrate, both displacement reactions are associated with the same or comparable energy barriers. Under certain conditions (here acidic pH), the equilibrium may be favorable for detection of intermediate state(s). We conclude that the previously reported apparent burst kinetics[18] resulted primarily from incorrect information regarding the catalytic activity of EcAII(T89V), while the failure of detecting AEI[20] was a consequence of using L-Asn (instead of L-Asp) as the substrate. It is necessary to point out that the experiments conducted in this study do not allow for detection of burst effects that typically extends over an initial microsecond to millisecond period. We eliminated only the previously suggested possibility of a "long unusual" burst effect.[18]

Tetrahedral Intermediate. In a series of LC-MS experiments (Figure 5b), we observed a gradual increase of the relative abundance of AEI with a decrease in pH. In parallel with these experiments, we performed structural studies of EcAII(K162M) crystals grown at different pH values in the presence of L-Asp. We observed that, at pH >5.6−5.8, only noncovalent complexes are seen (see Figure 2b and structures **6** and **9**). Decreasing the pH to approximately 5.2−5.5 results in the formation of AEI (Figure 2c). At pH 5.0, however, the difference electron density peak in the active site pocket could not be modeled by the noncovalent complex, AEI, or its combination with the substrate. This electron density could, however, be modeled by a mixture of AEI and TI at comparable occupancies. Panels a and b of Figure S8 provide support for incorporation of the composite model of the covalently bound substrate. The model of the active site with the TI component is presented in Figure 2e, while the complete refined model of the active site, consisting of both AEI and TI, is shown in Figure 2f. The agreement between this model and the electron density maps is illustrated in Figure S7. This structure represents a static snapshot of the catalytic reaction with L-Asp as the substrate. As mentioned in the introductory section, the exchange of catalytic oxygen for L-Asp is a reversible process in which only one TI is formed, equivalent to TI2 in hydrolysis of L-Asn. Thus, unless oxygen exchange in L-Asp follows a mechanism different from the hydrolysis of L-Asn (following Ehrman et al.,[15] such a scenario is very unlikely), structures of both tetrahedral intermediates in the latter reaction must be nearly identical. A network of interactions (primarily H-bonds) between TI and the catalytic pocket is illustrated in Figure 2e. A comparison with AEI shown in Figure 2c indicates no significant changes to this network. The same conclusion is apparent from a comparison of the relative positions of AEI and TI in the active site pocket, illustrated in Figure 2f. However, as mentioned above, a substrate was not significantly reoriented during conversion to AEI (Figure 2d). Three structures (noncovalent complex, TI, and AEI) outline the reaction pathway and indicate only minor conformational changes to the substrate throughout the catalytic process. The fixed orientation of the α-carboxyl group of the substrate (Figure 2d,f) supports our earlier conclusion about its central role in controlling binding affinity. Although the TI structure was observed for the complex with L-Asp where only a single TI is formed, the latter is also the best template for analysis of the interactions between the first TI1 in the reaction with L-Asn.

Efficient catalysis requires that the free energy of each TI be minimized through a specific set of interactions. For enzymes that catalyze hydrolysis by creating an intermediate tetrahedral intermediate, i.e., Ser/Cys proteases or proteasome,[3] a structural motif called the oxyanion hole has long been recognized as being central to stabilization of the negative charge of TI. However, in EcAII, the oxyanion hole has an unusual composition, being formed by two backbone amides (Thr12 and Ala114) and by the invariant w1. On the basis of the pattern of H-bonds (see Figure 4a, Figure S9, and the Supporting Information), this water projects one of its protons toward the $O_{\delta 1}^{-}$ atom of TI. The H-bond between w1 and TI($O_{\delta 1}^{-}$) rationalizes structural conservation of this water and its significance for catalysis. The $O_{\delta 2}$ atom in TI2 or the leaving group (NH_2 in L-Asn and $O_{\delta 2}$ in L-Asp) in TI1 is engaged in a set of three H-bonds with defined polarities, arranged in a nearly perfect tetrahedral configuration. In one of these H-bonds, the leaving group acts as the H-donor to the backbone carbonyl of Ala114, and in the second, it accepts a proton from Thr89(OH). The polarity of the third H-bond, which is the longest of the three and formed with an adjacent water molecule, is different in the case of NH_2 (donor) or $O_{\delta 2}$ (acceptor). In that state, the leaving group (a primary amine in

https://dx.doi.org/10.1021/acs.biochem.0c00116
Biochemistry 2020, 59, 1927−1945

the case of L-Asn or the hydroxyl in the case of L-Asp) extracts a proton from Lys162. The latter is less basic than a typical primary amine (due to protonation of the adjacent Asp90) and is more prone to donate a proton to the leaving group, via Thr89. This event changes the polarity of the H-bond between Lys162 and Thr89, from Lys162-NH···Thr89 to Lys162···HO-Thr89. The resulting first product (NH_3 or H_2O) diffuses out of the active site pocket and, likely, quickly becomes protonated. At this stage, Lys162 is in a transiently uncharged state and recaptures a proton from w2. That event reverses the polarity of the H-bond between Lys162 and Thr89, presenting the hydroxyl proton of the latter to a potential acceptor. An obligatory acceptor created in this event is w2($\rightarrow OH^-$).

The proton transfer events described above cannot be deciphered unambiguously from structural data, and the actual sequence of events may be somewhat different. For instance, uncharged Lys162 may extract a proton from Thr89, which subsequently recaptures it from w2 (this is the scheme used in QM calculations described below). However, the overall result is the same; i.e., w2 supplies a proton to neutral Lys162. The w2($\rightarrow OH^-$) shifts toward the hydroxyl proton of Thr89 (guided by the H-bond interaction) and is placed in an optimal position for the second nucleophilic attack on the C_γ atom of the now created AEI. The second intermediate, TI2, formed in this process, corresponds to TI observed in structures **2** and **3**, described in this report. At this point, the reaction proceeds along the lowest-energy path; i.e., a proton from Asp90 (originally sequestered from the nucleophilic Thr12) is relayed to its original location via an H-bond network of active site water molecules and Tyr25(OH). While this proton is being accepted by Thr12, the covalent linkage with the product is weakening and the change in hybridization from sp^2 to sp^3 leads to a change in the geometry of the resulting carboxyl group and its deprotonation. At that stage, the two effects contribute to the repulsion of the L-Asp product from the active site pocket, the reemergence of two negatively charged groups, and the repulsion of carboxyl groups (Asp90 and the α-carboxyl of the product), as well as the negatively charged β-carboxyl of the product, repelled by the carbonyl oxygen of Ala114. After repelling the product, the active site of the enzyme is restored to the initial state, ready for the next catalytic cycle.

Protonation Status of the Active Site Groups in EcAII. In addition to establishing the stereochemical properties of the involved residues, formulation of a catalytic mechanism requires a plausible description of their protonation state. In EcAII and most other L-asparaginases, at least four groups are capable of changing their protonation state. In addition to Asp90 and Lys162 of the enzyme, they include α-amino and α-carboxyl groups of the substrate, L-Asn. The side chain of Glu283 (contributed by the intimate protomer) is not considered because this residue is not conserved among L-asparaginases. When considering L-Asp as the substrate, we must also account for protonation of the side chain. Currently, there are no experimental data defining the protonation state of any of these groups; however, it is possible to present a plausible prediction based on the available structural and functional data for these enzymes, as well as on rules of general chemistry (i.e., ref 56). Subsequent characterization refers primarily to the enzyme (or its complex with a substrate) prior to the catalytic reaction. However, we will try to account for changes in the protonation states during catalysis.

In the ligand-free state, the active site of EcAII is exposed to the solvent and remains well hydrated even upon binding a substrate molecule (Figure 2a,b). Therefore, under physiological conditions, the K_a values of both Asp90 and Lys162 should not be very different from those determined for free amino acids in water[52] and both residues should be charged. For the same reason, α-amino and α-carboxyl groups of a substrate molecule should be charged. An alteration to this state may be expected upon substrate binding and, as we suggested earlier, with two negatively charged carboxylates forming a proton sink and Asp90 accepting the proton donated by the nucleophilic Thr12.

The two reports that argued against the double-displacement mechanism[19,20] assumed that Lys162 is in an uncharged state. Subsequently, this led the authors to the conclusion that direct displacement correctly describes the catalytic reaction. The assumption regarding the protonation state of Lys162 was based on unpublished results mentioned in ref 18, but at least two other sources suggested that Lys162 exists in a charged state prior to the catalytic reaction. As shown by Röhm and Van Etten,[16] the catalytic properties of EcAII are only minimally altered within the pH range of 4−10. The presence of uncharged Lys162 at pH 4 is extremely unlikely if not impossible, requiring a change in pK_a of nearly 7 log units from its normal value. Also, the results of the high-throughput activity screen (see Figure S2) indicate that K162R is the only variant retaining significant activity compared to EcAII(wt) (∼20%).

Protonation of Asp90 likely leads to a decrease in the pK_a value of Lys162, rendering it more prone to expelling a proton. We also predict that the acidity of L-Asp (the product, or an alternative substrate in an oxygen exchange reaction) is decreased compared to the standard value in water, due to its location in the active site. In the *cat*+ bound state, the β-carboxyl of L-Asp points toward the carbonyl oxygen of Ala114, forming an assembly with an increased affinity for a proton, which is manifested by a previously noted increase in the pK_a of the β-carboxylate of L-Asp.[16]

Catalytic Mechanism of EcAII Based on Experimental Data. Binding of the substrate of L-asparaginase is primarily controlled by the interactions of its α-carboxyl group and leads to major conformational rearrangements, first of the HR region, followed by large movements and conformational stabilization of ASFL. The hydroxyl oxygen of Thr12 begins to form a covalent bond with the C_γ atom of the substrate, the process being driven primarily by electrostatic forces. This is made possible due to simultaneous extraction of a proton that is attracted to the proton sink (α-carboxylate of the substrate and Asp90), where it is delivered through a network of H-bonds composed of the hydroxyl group of the conserved Tyr25 and a chain of water molecules. Protonation of Asp90 increases the acidity of the adjacent Lys162, while binding of Thr12 to the substrate results in changes in the electronic and stereochemical properties of the carboxamide group of the substrate [hybridization changes from planar (sp^2) to tetrahedral (sp^3)]. The first tetrahedral intermediate (TI1) is formed and stabilized by an extensive H-bond network within the active site pocket, including the nonconventional oxyanion hole. The leaving group, now a primary amine, extracts a proton from the side chain of Lys162 and departs the active site as NH_3. This irreversible process concludes the first displacement reaction. As a result, Lys162 is transiently

https://dx.doi.org/10.1021/acs.biochem.0c00116
Biochemistry 2020, 59, 1927−1945

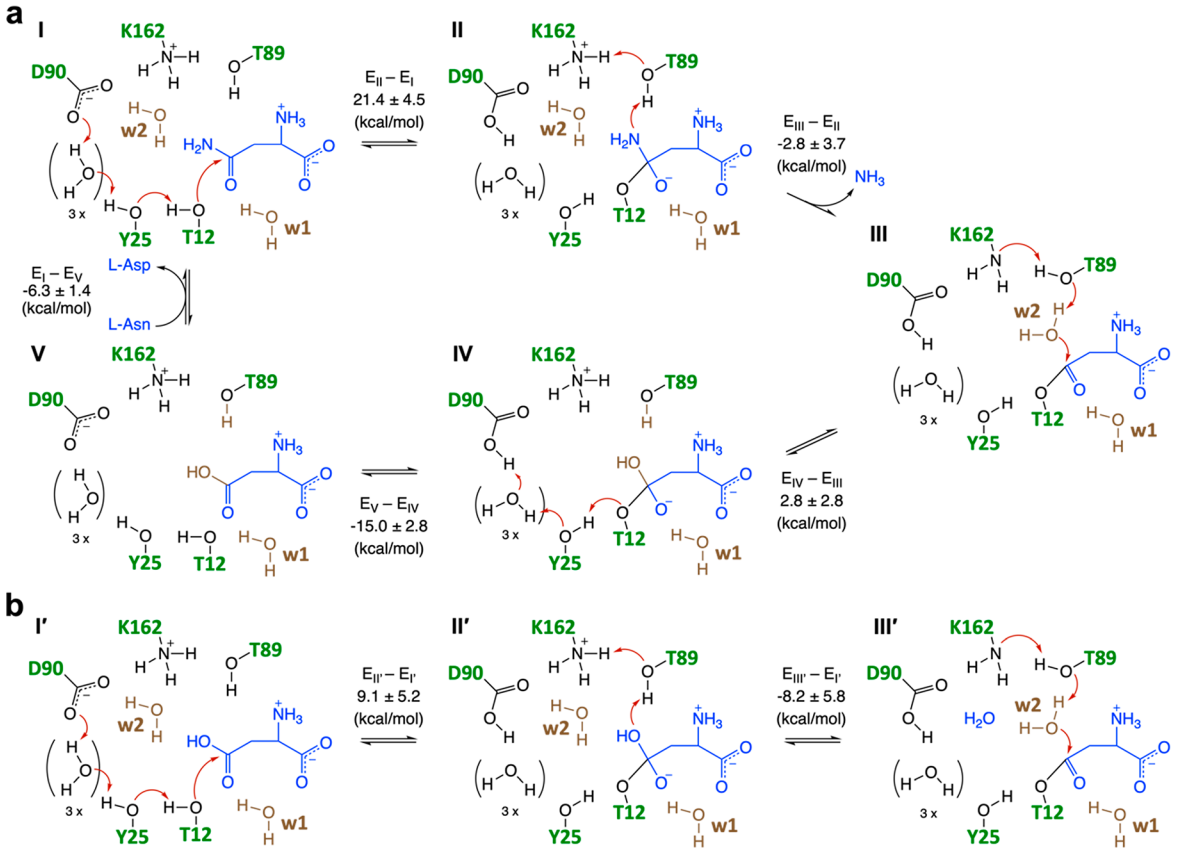

Figure 9. Schematic representation of the intermediate steps in the catalysis of (a) L-Asn and (b) L-Asp substrates. Average energy differences (computed with B3LYP, CAM-B3LYP, and ωB97X-D3 functionals with the aug-cc-pVDZ basis set) between steps of the cycle are shown.

uncharged and the ester group of AEI is shifted and rotated, compared to the substrate's carboxamide group.

Uncharged Lys162 extracts a proton from the highly conserved w2 via Thr89. Activated (or deprotonated, OH^-) w2, guided by an H-bond to Thr89, relocates to a position suitable for the second nucleophilic attack. This relocation of w2 is possible only after formation of AEI and its subsequent structural changes. The original site of w2 is most likely immediately replenished.

As a strong and well-positioned nucleophile, OH^- initiates the second displacement reaction leading to TI2, which is stereochemically indistinguishable from TI1. In the next step, the proton from Asp90 is transferred back to Thr12 through a network of active site water molecules and, finally, through Tyr25(OH). The covalent ester bond between Thr12 and the product is weakening. Hybridization and the geometry of TI2 are changing. The carboxyl group of the product is emerging. Finally, the hydrogen on the latter group is dissociating. This results in recovery of the original state of the active site of the enzyme, and the negatively charged product is expelled. Both HR and ASFL sections are converted into *cat*– conformations, primed for the next catalytic cycle. A scheme of the complete catalytic reaction is shown in Figure 9.

Support for the Catalytic Mechanism through Quantum Mechanical DFT Calculations. We tested the EcAII reaction mechanism using well-established quantum chemistry methods based on DFT. Due to the high computational cost of DFT, we selected a minimal subsystem of catalytic and essential structural amino acids near the active site that consists of 341 atoms and includes all of the catalytic residues (Thr12, Tyr25, Thr89, Asp90, and Lys162) and seven water molecules (including w1 and w2). We based our computational model on the structure of the complex between EcAII and L-Asp (PDB entry 6pac[30]). We tested the reaction mechanism with both L-Asn and L-Asp as substrates, to compare how the energetics of the reaction change depending on the substrate.

We have divided the reaction mechanism (Figure 9a) into five intermediate steps (I–V), starting with the bound substrate (I, L-Asn) and ending with the final product (V, L-Asp). To compute the energy differences between intermediate steps, we first optimized the structure of each intermediate with a small basis set [6-31G(d)] while fixing the positions of α-carbons (except for Gly11, Thr12, Ile13, Gly88, Thr89, and Asp90) to maintain the structural integrity of the active site. This step was followed by a single-point energy calculation with a larger and more accurate basis set (aug-cc-pVDZ). Successful optimization of all of the intermediate steps in the reaction indicates that each state is in a stable local energy minimum and does not transform spontaneously into another nearby lower-energy configuration. The observed energy differences between intermediate reaction steps are listed in Table 3, where we show energies computed with three functionals that vary in the treatment of long-range interactions (see Materials and Methods) to show the effect of the local protein environment on individual steps.

The first step of the reaction is the nucleophilic attack by Thr12(O_γ) on the C_γ atom of the substrate. This step is associated with the highest energy barrier, and it is likely the reaction rate-limiting step. The proton from Thr12 is

https://dx.doi.org/10.1021/acs.biochem.0c00116
Biochemistry 2020, 59, 1927–1945

Table 3. Energy Differences between Intermediate Reaction Steps of L-Asn (and L-Asp) Catalysis as Shown in Figure 9[a]

	B3LYP	CAM-B3LYP	ωB97X-D3	⟨ΔE⟩
$E_{II}-E_{I}$	25.9	21.2	17.0	21.4 ± 4.5
$E_{III}-E_{II}$	−6.9	0.2	−1.6	−2.8 ± 3.7
$E_{IV}-E_{III}$	6.1	0.9	1.5	2.8 ± 2.8
$E_{V}-E_{IV}$	−17.2	−16.0	−11.9	−15.0 ± 2.8
$E_{I}-E_{V}$	−7.8	−6.3	−5.0	−6.3 ± 1.4
$E_{II'}-E_{I'}$	14.7	8.0	4.5	9.1 ± 5.2
$E_{III'}-E_{II'}$	−14.8	−6.0	−3.8	−8.2 ± 5.8

[a]All systems were first optimized with the 6-31G(d) basis set, and final energies computed with the aug-cc-pVDZ basis set. All energies in kilocalories per mole.

transferred through Tyr25 and a network of H-bonded waters to the carboxyl group of Asp90. While we cannot determine the protonation state of Asp90 from the crystal structure, the H-bond between this residue and a neighboring water lies in the plane of the carboxyl group, an observation that may additionally indicate protonation of Asp90, as previously reported in other high-resolution structures.[57] This step is followed by acquisition of a proton from Lys162 through Thr89 and spontaneous cleavage and release of ammonia, leading to the formation of AEI (III). The coupling of pK_a's of protonated Asp90 and Lys162 was described earlier in this report. The II → III transition is favorable, as indicated by a decrease in energy of the system. Ejection of ammonia from the active site and reorientation of the C_γ moiety of the substrate create space for w2 to assume a position suitable for the second nucleophilic attack (III → IV), which proceeds through TI2 (IV). Enhancement of the nucleophilic properties of w2 was discussed earlier, and the computations indicate that, like the first nucleophilic attack, the second one is associated with an unfavorable increase in the system's energy, although now the energy barrier is much lower. The last step in the reaction (IV → V) involves spontaneous cleavage and subsequent release of the final product (L-Asp). During this step, Thr12 recaptures its proton from Asp90 through a network of H-bonded waters and Tyr25, utilized during the first displacement. This step is associated with a large decrease in the overall energy of the system.

Using the same approach, we computed the energy differences for the reaction of oxygen exchange with L-Asp as the substrate. Because this process is completely reversible (Figure 9b) and represents an equilibrium between the noncovalent EcAII:Asp complex and AEI, only two energy differences, associated with transformations of state I′ into state III′, were calculated (Figure 9b). Because of symmetry, energies describing the reverse reaction are the same. In the model utilized in our calculations, the side chain of the L-Asp substrate was protonated. In contrast to hydrolysis of L-Asn, the energy barrier associated with formation of TI is, as expected, significantly lower.

DISCUSSION

It has been known for more than 50 years that the enzymatic activity of L-asparaginases is associated with the significant anticancer properties of these enzymes, particularly for juvenile leukemia.[10] However, since the very beginning, questions about the mechanism of enzymatic activity have been raised, and the double-displacement scenario was considered as very plausible early on.[14,15] For almost three decades, the lack of experimental evidence prevented confirmation of any mechanistic hypotheses. Apparent progress was made in 1996, when the structure of the covalent acyl intermediate of EcAII was published,[18] but these results were not followed up. A few years ago, these early results were challenged on the basis of either theoretical calculations[19] or new experimental data.[20]

In this work, we aimed to provide a detailed description of all steps of the catalytic mechanism of L-asparaginases. We focused on EcAII because this most studied L-asparaginase is utilized as a crucial component of anticancer therapy of leukemias and lymphomas.[58] Although our data focus on EcAII variants, we believe that the results presented here can be extended to all type II L-asparaginases and, very likely, to type I L-asparaginases or their analogues from extremophiles. The latter suggestion, however, requires further confirmation.

The most critical evidence was obtained from crystal structures of several variants of EcAII in a ligand-free form or in complex with the substrates. We selected a subset of 11 structures that were most relevant to description of the catalytic mechanism. Other structures were published by us previously, in relation to different properties of EcAII.[30,41] The most compelling result was obtained during analysis of the structure of EcAII(K162M), crystallized in the presence of L-Asp at pH 5 (structures **2** and **3**). These structures revealed detailed descriptions of the active site occupied by either covalent AEI or TI. Structures with only AEI were determined for the same variant at pH 5.2 (structures **4** and **5**), as well as for other two variants, EcAII(T89V,K162T) (structures **7** and **8**) and EcAII(T89V).[18] In response to the earlier criticism,[20] crystals used for determinations of structures **4**, **5**, **7**, and **8** were prepared with particular care to minimize the possibility of non-enzymatic reaction. Crystals were soaked in solutions containing L-Asp for as little as 10 s prior to the collection of X-ray data. Assuming that the acetylation step is shorter than the crystal soaking time and much shorter than the deacetylation step (estimated from the k_{cat} to be in excess of 250 s), we expected accumulation of the acyl-enzyme intermediate.

Structures **2**−**5**, **7**, and **8** clearly indicate that Thr12 serves as the primary nucleophile, immediately implying that the catalytic reaction follows the double-displacement mechanism. It should be noted that all of these results were obtained with L-Asp as a substrate. These results could not be reproduced with L-Asn; however, an analysis presented here and the previously published results[55] lead to the conclusion that, in the canonical reaction (with L-Asn), the first (acylation) step controls the reaction rate. Under such conditions, AEI does not accumulate in quantities that could be detected by the currently employed methodology.

Compared to other enzymes catalyzing similar reactions, i.e., Ser/Cys proteases,[3] proteasomes, or acyltransferases,[59] the mechanism proposed here is significantly different. Despite the existence of the putative Asp90-Lys162-Thr89 active site triad in L-asparaginases (at first glance similar to that found in proteasomes and acyltransferases), the covalent AEI is formed with a different residue (Thr12), which is not in direct interaction with a general base. The explanation of this apparent puzzle stems from the coexistence of several simultaneous effects and/or states: (i) precise placement of a substrate molecule, (ii) a particular conformational change of the HR region, (iii) significant electrostatic force between the interacting atoms [Thr12(O_γ) and the C_γ atom of the substrate], and (iv) formation of the proton sink upon substrate binding.

https://dx.doi.org/10.1021/acs.biochem.0c00116
Biochemistry 2020, 59, 1927−1945

Two features, activation of nucleophilic threonine by a distant proton sink (a general base) and an unusual oxyanion hole, differentiate EcAII (and possibly all L-asparaginases) from other enzymes catalyzing similar reactions. The presence of an apparently typical catalytic triad is misleading as there is no evidence that this motif contributes a nucleophile in the acylation step. With the departure of NH_3, Lys162 becomes transiently neutral. However, it regains the preferred charged state by extraction of a proton from the adjacent w2, which together with w1 is conserved in all L-asparaginases. The resulting hydroxyl anion, aided by Thr89(OH), relocates into an optimal position for the second nucleophilic attack.

The proposed mechanism explains the role of five residues in the active site of EcAII (Thr12, Tyr25, Thr89, Asp90, and Lys162) that are invariant in L-asparaginases and critical for catalysis. This mechanism also predicts that mutations of Tyr25 and Thr89, residues acting primarily as proton conveyors, have a strong but not necessarily deleterious effect on the catalytic process. On the other hand, the primary nucleophile Thr12 and Lys162, critical for activating the water molecule responsible for the second nucleophilic attack, are both indispensable and, when mutated, render a nearly inactive enzyme. Asp90 plays a critical but more ambiguous role. This residue appears to be central for binding and assists with extraction of a proton from the primary nucleophile, playing the role of a general base. After subsequent protonation, it increases the acidity of the adjacent Lys162, thus influencing both steps of the double-displacement reaction. Within this scheme, it is also possible to explain the seemingly unusual activity of the D90K variant. Namely, the side chain of Lys90, similar in length to aspartate, is located in direct contact with the side chain of Lys162. It is thus quite plausible that the amino group of Lys90 is uncharged and capable of assuming the role of a general base, resulting in an enzyme that is somewhat catalytically deficient but still active.

We performed quantum mechanical calculations to verify the feasibility of the catalytic mechanism. All intermediate states of the reaction were associated with reasonable energy differences, supporting the proposed mechanism. The theoretical model of the active site comprised 341 atoms. During the theoretical studies of EcAII, we observed that the energy change associated with the I → II transition (Figure 9a) depends greatly (±10 kcal/mol) on the positions of H-bonded waters in the active site (Figure 2), which were derived from the structure of a single complex (PDB entry 6pac). Notably, the energy effects do not account for substrate binding and product release; however, they include other main events, such as the first nucleophilic attack by Thr12, a proton shuttle through Tyr25 and a network of waters, the role of Asp90 as a proton sink, and Lys162 as an activator of the second nucleophilic water.

Recently, different conclusions (favoring the single-displacement mechanism) were reported on the basis of both experimental studies[20] and theoretical calculations.[19] On the basis of new experimental structural and computational studies, we addressed here the most plausible reasons for the reported discrepancies. It is intriguing, however, why the theoretical evaluation of the catalytic process leads to such different conclusions when nearly identical structures of EcAII are used as templates. We believe that in the earlier studies,[19] a model of the EcAII active site was too extensively simplified and inadequate to account for all significant events. First, it incorporated only a single water molecule, but as we showed above, at least two active site water molecules are invariant in all structures of L-asparaginases and are accompanied by several additional, slightly less structurally conserved water molecules, which are critical for catalysis. As a result, decreasing the content of the active site to just one water molecule effectively eliminates the double-displacement mechanism. An assumption of the uncharged Lys162, central to the earlier calculations, is in serious disagreement with basic chemistry and the evidence from kinetic studies of EcAII variants. Finally, previous theoretical analysis completely disregarded the role of Tyr25 in catalysis. The analysis presented here is significantly more complete and consistent with the experimental results, as well as with general chemical rules.

Resolving the mechanism of catalysis by EcAII and, potentially, by other L-asparaginases provides a novel view of the nucleophilic substitution reaction that involves a weak nucleophile that is not assisted by a general base. Although L-asparaginases are very successfully used as a component of highly efficacious anticancer therapy, a continuing effort to develop new variants with a higher efficiency and weaker side effects is still ongoing. Detailed knowledge of the catalytic process will help in such explorations.

■ ASSOCIATED CONTENT

Supporting Information

The Supporting Information is available free of charge at https://pubs.acs.org/doi/10.1021/acs.biochem.0c00116.

Detailed data collection and refinement statistics, structure of the active site, biochemical characterization of the EcAII variants, high-throughput screening results, conformational changes during substrate binding, progress curves of substrate hydrolysis, electron density maps, and structure of the oxyanion hole and proton sink (PDF)

Architecture of L-asparaginase (AVI)

Binding of a substrate (AVI)

Conformational changes during substrate binding (AVI)

Accession Codes

EcAII, UniProtKB P00805; PDB entries 6v23, 6v2c, 6v2g, 6v24, 6v25, 6v26, 6v27, 6v28, 6v29, 6v2a, and6v2b.

■ AUTHOR INFORMATION

Corresponding Author

Jacek Lubkowski − *Macromolecular Crystallography Laboratory, Center for Cancer Research, National Cancer Institute, Frederick, Maryland 21702, United States;* orcid.org/0000-0002-8673-6347; Email: lubkowsj@mail.nih.gov

Authors

Juan Vanegas − *Department of Physics, The University of Vermont, Burlington, Vermont 05408, United States;* orcid.org/0000-0003-1381-1649

Wai-Kin Chan − *Department of Bioinformatics and Computational Biology, The University of Texas M. D. Anderson Cancer Center, Houston, Texas 77030, United States*

Philip L. Lorenzi − *Department of Bioinformatics and Computational Biology, The University of Texas M. D. Anderson Cancer Center, Houston, Texas 77030, United States;* orcid.org/0000-0003-0385-7774

https://dx.doi.org/10.1021/acs.biochem.0c00116
Biochemistry 2020, 59, 1927−1945

John N. Weinstein − *Department of Bioinformatics and Computational Biology, The University of Texas M. D. Anderson Cancer Center, Houston, Texas 77030, United States*
Sergei Sukharev − *Department of Biology, University of Maryland, College Park, Maryland 20742, United States;* orcid.org/0000-0002-4807-9665
David Fushman − *Department of Chemistry and Biochemistry, University of Maryland, College Park, Maryland 20742, United States;* orcid.org/0000-0002-6634-8056
Susan Rempe − *Center for Biological and Engineering Sciences, Sandia National Laboratories, Albuquerque, New Mexico 87185, United States*
Andriy Anishkin − *Department of Biology, University of Maryland, College Park, Maryland 20742, United States*
Alexander Wlodawer − *Macromolecular Crystallography Laboratory, Center for Cancer Research, National Cancer Institute, Frederick, Maryland 21702, United States;* orcid.org/0000-0002-5510-9703

Complete contact information is available at: https://pubs.acs.org/10.1021/acs.biochem.0c00116

Funding

This project has been funded in part by the Intramural Research Program of the National Institutes of Health (NIH), National Cancer Institute, Center for Cancer Research. NMR instrumentation was supported in part by National Science Foundation Grant DBI1040158. Additional support was provided by Cancer Prevention and Research Institute of Texas Grant RP130397 and NIH Grants S10OD012304-01, U01CA235510, and P30CA016672.

Notes

The authors declare no competing financial interest.

■ ACKNOWLEDGMENTS

The authors thank Dr. Di Zhang for help in purification of the samples of EcAII used in crystallization and kinetics studies. Sandia National Laboratories is a multimission laboratory managed and operated by National Technology and Engineering Solutions of Sandia, LLC, a wholly owned subsidiary of Honeywell International, Inc., for the U.S. Department of Energy's NNSA under Contract DE-NA-0003525. This work was supported by Sandia's LDRD program and performed, in part, at the Center for Integrated NanoTechnology (CINT). This paper describes objective technical results and analysis. Any subjective views or opinions that might be expressed in the paper do not necessarily represent the views of the U.S. DOE or the U.S. Government.

■ REFERENCES

(1) Wriston, J. C. (1985) Asparaginase. In *Methods of Enzymology*, pp 608−618, Academic Press.
(2) Batool, T., Makky, E. A., Jalal, M., and Yusoff, M. M. (2016) A comprehensive review on L-asparaginase and its applications. *Appl. Biochem. Biotechnol. 178*, 900−923.
(3) Hedstrom, L. (2002) Serine protease mechanism and specificity. *Chem. Rev. 102*, 4501−4524.
(4) Epp, O., Steigemann, W., Formanek, H., and Huber, R. (1971) Crystallographic evidence for the tetrameric subunit structure of L-asparaginase from *Escherichia coli*. *Eur. J. Biochem. 20*, 432−437.
(5) Swain, A. L., Jaskólski, M., Housset, D., Rao, J. K. M., and Wlodawer, A. (1993) Crystal structure of *Escherichia coli* L-asparaginase, an enzyme used in cancer therapy. *Proc. Natl. Acad. Sci. U. S. A. 90*, 1474−1478.
(6) Bansal, S., Gnaneswari, D., Mishra, P., and Kundu, B. (2010) Structural stability and functional analysis of L-asparaginase from *Pyrococcus furiosus*. *Biochemistry (Moscow) 75*, 375−381.
(7) Broome, J. D. (1961) Evidence that the L-asparaginase activity of guinea pig serum is responsible for its antilymphoma effects. *Nature 191*, 1114−1115.
(8) Brumano, L. P., da Silva, F. V. S., Costa-Silva, T. A., Apolinario, A. C., Santos, J., Kleingesinds, E. K., Monteiro, G., Rangel-Yagui, C. O., Benyahia, B., and Junior, A. P. (2019) Development of L-asparaginase biobetters: current research status and review of the desirable quality profiles. *Front. Bioeng. Biotechnol. 6*, 212.
(9) Lomelino, C. L., Andring, J. T., McKenna, R., and Kilberg, M. S. (2017) Asparagine synthetase: Function, structure, and role in disease. *J. Biol. Chem. 292*, 19952−19958.
(10) Koprivnikar, J., McCloskey, J., and Faderl, S. (2017) Safety, efficacy, and clinical utility of asparaginase in the treatment of adult patients with acute lymphoblastic leukemia. *OncoTargets Ther. 10*, 1413−1422.
(11) Chan, W. K., Horvath, T. D., Tan, L., Link, T., Harutyunyan, K. G., Pontikos, M. A., Anishkin, A., Du, D., Martin, L. A., Yin, E., Rempe, S. B., Sukharev, S., Konopleva, M., Weinstein, J. N., and Lorenzi, P. L. (2019) Glutaminase activity of L-asparaginase contributes to durable preclinical activity against acute lymphoblastic leukemia. *Mol. Cancer Ther. 18*, 1587−1592.
(12) Kornbrust, B. A., Stringer, M. A., Lange, N. E., and Hendriksen, H. V. (2009) Asparaginase: An Enzyme for Acrylamide Reduction in Food Products. In *Enzymes in Food Technology* (Whitehurst, R. J., and van Oort, J., Eds.) pp 59−87.
(13) Mashburn, L. T., and Wriston, J. C. (1964) Tumor inhibitory effect of L-asparaginase from *Escherichia coli*. *Arch. Biochem. Biophys. 105*, 450−452.
(14) Röhm, K. H., and Schneider, F. (1971) Kinetische Untersuchungen zum Mechanismus der Asparaginase aus *E. coli*. *Hoppe Seyler's Z. Physiol. Chem. 352*, 1739−1743.
(15) Ehrman, M., Cedar, H., and Schwartz, J. H. (1971) L-asparaginase II of *Escherichia coli*, studies on the mechanism of action. *J. Biol. Chem. 246*, 88−94.
(16) Röhm, K. H., and Van Etten, R. L. (1986) The ^{18}O isotope effect in ^{13}C nuclear magnetic resonance spectroscopy: mechanistic studies on asparaginase from *Escherichia coli*. *Arch. Biochem. Biophys. 244*, 128−136.
(17) Miller, M., Rao, J. K. M., Wlodawer, A., and Gribskov, M. R. (1993) A left-handed crossover involved in amidohydrolase catalysis. Crystal structure of *Erwinia chrysanthemi* L-asparaginase with bound L-aspartate. *FEBS Lett. 328*, 275−279.
(18) Palm, G. J., Lubkowski, J., Derst, C., Schleper, S., Röhm, K. H., and Wlodawer, A. (1996) A covalently bound catalytic intermediate in *Escherichia coli* asparaginase: crystal structure of a Thr-89-Val mutant. *FEBS Lett. 390*, 211−216.
(19) Gesto, D. S., Cerqueira, N. M., Fernandes, P. A., and Ramos, M. J. (2013) Unraveling the enigmatic mechanism of L-asparaginase II with QM/QM calculations. *J. Am. Chem. Soc. 135*, 7146−7158.
(20) Schalk, A. M., Antansijevic, A., Caffrey, M., and Lavie, A. (2016) Experimental data in support of a direct displacement mechanism for Type I/II L-asparaginases. *J. Biol. Chem. 291*, 5088−5100.
(21) Chan, W. K., Lorenzi, P. L., Anishkin, A., Purwaha, P., Rogers, D. M., Sukharev, S., Rempe, S. B., and Weinstein, J. N. (2014) The glutaminase activity of L-asparaginase is not required for anticancer activity against ASNS-negative cells. *Blood 123*, 3596−3606.
(22) Minor, W., Cymborowski, M., Otwinowski, Z., and Chruszcz, M. (2006) HKL-3000: The integration of data reduction and structure solution - from diffraction images to an initial model in minutes. *Acta Crystallogr., Sect. D: Biol. Crystallogr. D62*, 859−866.
(23) McCoy, A. J., Grosse-Kunstleve, R. W., Adams, P. D., Winn, M. D., Storoni, L. C., and Read, R. J. (2007) *Phaser* crystallograhic software. *J. Appl. Crystallogr. 40*, 658−674.
(24) Murshudov, G. N., Skubak, P., Lebedev, A. A., Pannu, N. S., Steiner, R. A., Nicholls, R. A., Winn, M. D., Long, F., and Vagin, A. A.

(2011) REFMAC5 for the refinement of macromolecular crystal structures. *Acta Crystallogr., Sect. D: Biol. Crystallogr. D67*, 355−367.
(25) Emsley, P., and Cowtan, K. (2004) Coot: model-building tools for molecular graphics. *Acta Crystallogr., Sect. D: Biol. Crystallogr. D60*, 2126−2132.
(26) Chen, V. B., Arendall, W. B., III, Headd, J. J., Keedy, D. A., Immormino, R. M., Kapral, G. J., Murray, L. W., Richardson, J. S., and Richardson, D. C. (2010) MolProbity: all-atom structure validation for macromolecular crystallography. *Acta Crystallogr., Sect. D: Biol. Crystallogr. 66*, 12−21.
(27) Derst, C., Henseling, J., and Röhm, K. H. (1992) Probing the role of threonine and serine residues of *E. coli* asparaginase II by site-specific mutagenesis. *Protein Eng., Des. Sel. 5*, 785−789.
(28) Frear, D. S., and Burrell, R. C. (1955) Spectrophotometric method for determining hydroxylamine reductase activity in higher plants. *Anal. Chem. 27*, 1664−1665.
(29) Shao, Y., Gan, Z., Epifanovsky, E., Gilbert, A. T. B., Wormit, M., Kussmann, J., Lange, A. W., Behn, A., Deng, J., Feng, X., Ghosh, D., Goldey, M., Horn, P. R., Jacobson, L. D., Kaliman, I., Khaliullin, R. Z., Kuś, T., Landau, A., Liu, J., Proynov, E. I., Rhee, Y. M., Richard, R. M., Rohrdanz, M. A., Steele, R. P., Sundstrom, E. J., Woodcock, H. L., Zimmerman, P. M., Zuev, D., Albrecht, B., Alguire, E., Austin, B., Beran, G. J. O., Bernard, Y. A., Berquist, E., Brandhorst, K., Bravaya, K. B., Brown, S. T., Casanova, D., Chang, C.-M., Chen, Y., Chien, S. H., Closser, K. D., Crittenden, D. L., Diedenhofen, M., DiStasio, R. A., Do, H., Dutoi, A. D., Edgar, R. G., Fatehi, S., Fusti-Molnar, L., Ghysels, A., Golubeva-Zadorozhnaya, A., Gomes, J., Hanson-Heine, M. W. D., Harbach, P. H. P., Hauser, A. W., Hohenstein, E. G., Holden, Z. C., Jagau, T.-C., Ji, H., Kaduk, B., Khistyaev, K., Kim, J., Kim, J., King, R. A., Klunzinger, P., Kosenkov, D., Kowalczyk, T., Krauter, C. M., Lao, K. U., Laurent, A. D., Lawler, K. V., Levchenko, S. V., Lin, C. Y., Liu, F., Livshits, E., Lochan, R. C., Luenser, A., Manohar, P., Manzer, S. F., Mao, S.-P., Mardirossian, N., Marenich, A. V., Maurer, S. A., Mayhall, N. J., Neuscamman, E., Oana, C. M., Olivares-Amaya, R., O'Neill, D. P., Parkhill, J. A., Perrine, T. M., Peverati, R., Prociuk, A., Rehn, D. R., Rosta, E., Russ, N. J., Sharada, S. M., Sharma, S., Small, D. W., Sodt, A., Stein, T., Stück, D., Su, Y.-C., Thom, A. J. W., Tsuchimochi, T., Vanovschi, V., Vogt, L., Vydrov, O., Wang, T., Watson, M. A., Wenzel, J., White, A., Williams, C. F., Yang, J., Yeganeh, S., Yost, S. R., You, Z.-Q., Zhang, I. Y., Zhang, X., Zhao, Y., Brooks, B. R., Chan, G. K. L., Chipman, D. M., Cramer, C. J., Goddard, W. A., Gordon, M. S., Hehre, W. J., Klamt, A., Schaefer, H. F., Schmidt, M. W., Sherrill, C. D., Truhlar, D. G., Warshel, A., Xu, X., Aspuru-Guzik, A., Baer, R., Bell, A. T., Besley, N. A., Chai, J.-D., Dreuw, A., Dunietz, B. D., Furlani, T. R., Gwaltney, S. R., Hsu, C.-P., Jung, Y., Kong, J., Lambrecht, D. S., Liang, W., Ochsenfeld, C., Rassolov, V. A., Slipchenko, L. V., Subotnik, J. E., Van Voorhis, T., Herbert, J. M., Krylov, A. I., Gill, P. M. W., and Head-Gordon, M. (2015) Advances in molecular quantum chemistry contained in the Q-Chem 4 program package. *Mol. Phys. 113*, 184−215.
(30) Lubkowski, J., and Wlodawer, A. (2019) Geometric considerations support the double-displacement catalytic mechanism of L-asparaginase. *Protein Sci. 28*, 1850−1864.
(31) Becke, A. D. (1993) Density-functional thermochemistry. III. The role of exact exchange. *J. Chem. Phys. 98*, 5648−5652.
(32) Lee, C., Yang, W., and Parr, R. G. (1988) Development of the Colle-Salvetti correlation-energy formula into a functional of the electron density. *Phys. Rev. B: Condens. Matter Mater. Phys. 37*, 785−789.
(33) Stephens, P. J., Devlin, F. J., Chabalowski, C. F., and Frisch, M. J. (1994) Ab initio calculation of vibrational absorption and circular dichroism spectra using density functional force fields. *J. Phys. Chem. 98*, 11623−11627.
(34) Yanai, T., Tew, D. P., and Handy, N. C. (2004) A new hybrid exchange−correlation functional using the Coulomb-attenuating method (CAM-B3LYP). *Chem. Phys. Lett. 393*, 51−57.
(35) Lin, Y. S., Li, G. D., Mao, S. P., and Chai, J. D. (2013) Long-range corrected hybrid density functionals with improved dispersion corrections. *J. Chem. Theory Comput. 9*, 263−272.
(36) Chai, J. D., and Head-Gordon, M. (2008) Long-range corrected hybrid density functionals with damped atom-atom dispersion corrections. *Phys. Chem. Chem. Phys. 10*, 6615−6620.
(37) Cox, S. R., and Williams, D. E. (1981) Representation of the molecular electrostatic potential by a net atomic charge model. *J. Comput. Chem. 2*, 304−323.
(38) Chirlian, L. E., and Francl, M. M. (1987) Atomic charges derived from electrostatic potentials: A detailed study. *J. Comput. Chem. 8*, 894−905.
(39) Breneman, C. M., and Wiberg, K. B. (1990) Determining atom-centered monopoles from molecular electrostatic potentials. The need for high sampling density in formamide conformational analysis. *J. Comput. Chem. 11*, 361−373.
(40) Herbert, J. M., Jacobson, L. D., Un Lao, K., and Rohrdanz, M. A. (2012) Rapid computation of intermolecular interactions in molecular and ionic clusters: self-consistent polarization plus symmetry-adapted perturbation theory. *Phys. Chem. Chem. Phys. 14*, 7679−7699.
(41) Lubkowski, J., Chan, W., and Wlodawer, A. (2019) Opportunistic complexes of *E. coli* L-Asparaginases with citrate anions. *Sci. Rep. 9*, 11070.
(42) Aghaiypour, K., Wlodawer, A., and Lubkowski, J. (2001) Do L-asparaginases utilize a catalytic triad Thr-Tyr-Glu? *Biochim. Biophys. Acta, Protein Struct. Mol. Enzymol. 1550*, 117−129.
(43) Aghaiypour, K., Wlodawer, A., and Lubkowski, J. (2001) Structural basis for the activity and substrate specificity of *Erwinia chrysanthemi* L-asparaginase. *Biochemistry 40*, 5655−5664.
(44) Derst, C., Wehner, A., Specht, V., and Röhm, K. H. (1994) States and functions of tyrosine residues in Escherichia coli asparaginase II. *Eur. J. Biochem. 224*, 533−540.
(45) Derst, C. (1995) Untersuchungen zur stabilitat und veranderung der substratspezfitat der L-asparaginase II aus Escherichia coli und klonierung und sequenzierung der L-asparaginase aus Wolinella succinogenes. Ph.D. Thesis, Philipps-Universitat, Marburg (Lahn), Germany.
(46) Aung, H. P. (1997) Directed mutagenesis of active-site residues of *E. coli* asparaginase II: Characterisation of the mutants by steady-state and pre-steady state kinetics and stability studies. Ph.D. Thesis, Philipps-Universitat, Marburg (Lahn), Germany.
(47) Schleper, S. (1999) Kinetische Untersuchungen und Modellstudien zur Funktion essentieller Reste im aktiven Zentrum der L-Asparaginase II aus *E.coli*. Ph.D. Thesis, Philipps-Universitat, Marburg (Lahn), Germany.
(48) Derst, C., Henseling, J., and Röhm, K. H. (2000) Engineering the substrate specificity of *Escherichia coli* asparaginase. II. Selective reduction of glutaminase activity by amino acid replacements at position 248. *Protein Sci. 9*, 2009−2017.
(49) Lubkowski, J., Palm, G. J., Gilliland, G. L., Derst, C., Röhm, K. H., and Wlodawer, A. (1996) Crystal structure and amino acid sequence of *Wolinella succinogenes* L-asparaginase. *Eur. J. Biochem. 241*, 201−207.
(50) Lubkowski, J., Wlodawer, A., Ammon, H. L., Copeland, T. D., and Swain, A. L. (1994) Structural characterization of *Pseudomonas 7A* glutaminase-asparaginase. *Biochemistry 33*, 10257−10265.
(51) Nguyen, H. A., Durden, D. L., and Lavie, A. (2017) The differential ability of asparagine and glutamine in promoting the closed/active enzyme conformation rationalizes the Wolinella succinogenes L-asparaginase substrate specificity. *Sci. Rep. 7*, 41643.
(52) Lide, D. R. (1991) *Handbook of Chemistry and Physics*, 72nd ed., CRC Press, Inc., Boca Raton, FL.
(53) Strohmeier, M., Stueber, D., and Grant, D. M. (2003) Accurate (13)C and (15)N chemical shift and (14)N quadrupolar coupling constant calculations in amino acid crystals: Zwitterionic, hydrogen-bonded systems. *J. Phys. Chem. A 107*, 7629−7642.
(54) Arnold, W. D., Sanders, L. K., McMahon, M. T., Volkov, A. V., Wu, G., Coppens, P., Wilson, S. R., Godbout, N., and Oldfield, E. (2000) Experimental, hartree−fock, and density functional theory investigations of the charge density, dipole moment, electrostatic

https://dx.doi.org/10.1021/acs.biochem.0c00116
Biochemistry 2020, 59, 1927−1945

potential, and electric field gradients in L-asparagine monohydrate. *J. Am. Chem. Soc. 122*, 4708−4717.
(55) Herrmann, V., Röhm, K. H., and Schneider, F. (1974) On the substrate specificity of L-asparaginase from *E. coli*. *FEBS Lett. 39*, 214−217.
(56) Isom, D. G., Castaneda, C. A., Cannon, B. R., and Garcia-Moreno E., B. (2011) Large shifts in pKa values of lysine residues buried inside a protein. *Proc. Natl. Acad. Sci. U. S. A. 108*, 5260−5265.
(57) Fisher, S. J., Blakeley, M. P., Cianci, M., McSweeney, S., and Helliwell, J. R. (2012) Protonation-state determination in proteins using high-resolution X-ray crystallography: effects of resolution and completeness. *Acta Crystallogr., Sect. D: Biol. Crystallogr. D68*, 800−809.
(58) Egler, R. A., Ahuja, S. P., and Matloub, Y. (2016) L-asparaginase in the treatment of patients with acute lymphoblastic leukemia. *J. Pharmacol. Pharmacother. 7*, 62−71.
(59) Marc, F., Weigel, P., Legrain, C., Almeras, Y., Santrot, M., Glansdorff, N., and Sakanyan, V. (2000) Characterization and kinetic mechanism of mono- and bifunctional ornithine acetyltransferases from thermophilic microorganisms. *Eur. J. Biochem. 267*, 5217−5226.

https://dx.doi.org/10.1021/acs.biochem.0c00116
Biochemistry 2020, 59, 1927−1945